DEMOCRATIC AND POPULAR ALGERIAN REPUBLIC

Ministry of Higher Education and Scientific Research

CSA CENTRE SIDI ABDELLAH CANCEROLOGIE

جامعة البليدة 1 UNIVERSITE BLIDA 1

Validation of bladder preparation in prostate radiotherapy

Master's Thesis in Medical Physics

Presented by:

MERZOUG Abdelhakim MAMACHE Abdellah

Presented before the members of the jury :

Mr. D. BARA	MRA	CDTA-Algiers	President
Mr. M. LAOUES	MCB	U. S. D.-Blida 1	Examiner
Mr. A. SIDI MOUSSA	Senior Medical Physicist	CSA-Algiers	Supervisor

Department of Physics

Faculty of Science

University of SAAD DAHLEB

BLIDA

July 2, 2024

Abstract

Purpose: Tomotherapy relies heavily on consistent patient preparation to ensure accurate treatment delivery. This study assesses the effectiveness of a preparation protocol by analyzing variations in bladder and evaluating impact of poor preparations among patients undergoing tomotherapy.

Methods: This study involved two study cases focused on prostate tomotherapy. The first case included 10 patients who received hypofractionated treatment whose dose volumes were computed for each fraction by experienced physicists using the TomoTherapy planning system. Bladder contours and dose computations were performed by supervised medical physicist students which involved contouring the bladder across multiple MegaVoltage Computed Tomography (MVCT) scans, yielding over 200 bladder contours using RayStation™ and Planned Adaptive™. The second case surveyed 24 patients on treatment preparation. Computed Tomography (CT) images from treatment sessions were registered with planning CT. Bladder contours were contoured and were used to calculate verification doses in Planned Adaptive™. Summation doses were assessed and compared to planning doses using Dose-volume histograms (DVHs). Exported summation doses, planning doses, CT images, and contours were analyzed using Python. The analysis included computing bladder volumes, constructing DVHs, and performing regression analyses to explore correlations among parameters.

Results: All patients, except one, exhibited significant dose volume inter-fraction differences between initial planning and poor preparation, both in low and high dose regions. Re-preparations significantly reduced these differences. Some planning preparations could have matched the optimal preparations.

Dose volume metrics showed an average inter-fraction difference, with bladder volume increases of 18.48% at 2.04 Gy, 13.68% at 2.43 Gy, and 1.2% at 3 Gy. Comparing bladder volumes, there was a 53.5% decrease between planning and poor preparations, and re-preparations increased bladder volume by 8.09%, while optimal preparations increased it by 30.39%.

An exponential regression model given by the expression $D_{mean} = 2.09e^{-0.005V}$ explained 77.33% of the variance in the mean bladder dose.

Summation dose indicated six patients with DVH metrics exceeding planning, with two exceeding constraints, while three had met the constraints. One patient had alternating DVH metrics, and one of the patients benefited from re-preparations that lowered metrics below constraints. A linear increase in the number of acceptable poor preparations was observed with increasing planning bladder volume, becoming fully acceptable at 398.61

cubic centimeters (cc).
Due to missing bladder volume data in the second study case, the sample size was smaller than expected, with only 2 out of 28 samples having complete data. High variance in bladder filling patterns was observed, with an R^2 score of 0.1724, not aligning with the expected pattern.

Conclusion: The results demonstrated that all well-prepared patients met the treatment constraints. Other findings showed that thorough bladder preparation before planning is crucial, as it significantly impacts the effectiveness and accuracy of subsequent treatments.

Contents

Abstract **1**

Acronyms **4**

1 Introduction **5**

1.1 Overview 5

1.2 Objectives 5

1.3 Limitations 6

2 Literature review **7**

2.1 Prostate Cancer 7

2.1.1 Prostate gland 7

2.1.2 Epidemiology 7

2.1.3 Types of prostate cancer 10

2.1.4 Diagnosis and Staging 10

2.1.5 Treatment 11

2.2 Interaction photons matter 12

2.2.1 Compton Scattering 12

2.2.2 Photoelectric effect 12

2.2.3 The relative importance of types of interaction at 6 MeV 13

2.2.4 Attenuation of photons within materials 13

2.3 Radiotherapy 15

2.3.1 Intensity-modulated radiation therapy 15

2.3.2 Image-guided radiation therapy 16

2.3.3 Tomotherapy 17
2.3.4 Radiotherapy workflow 19
2.3.5 Dose Volume Histogram 22

3 Materials and methodologies 23
3.1 Materials description 23
3.1.1 Dose constraints and objectives 24
3.2 Patient preparation 24
3.3 Dose calculation 25
3.3.1 IVDT 25
3.3.2 Contouring and Segmentation 28
3.3.3 Verification and Summation dose calculation 29
3.4 Dose-volume variation analysis 30

4 Results 31
4.1 First study case : Dose-volume variation analysis 31
4.1.1 Inter-fraction DVH Comparison 31
4.1.2 Correlation between dose and volume 35
4.1.3 Summation DVH Comparison 37
4.1.4 Impact of poor simulation preparations 41
4.2 Second study case : Patients survey 45

5 Discussions and conclusion 47
5.1 Discussion of results 47
5.2 Conclusion 48
5.3 Future work 48

Acknowledgements 49

Bibliography 51

Acronyms

3D threedimensional. 15

3D-CRT threedimensional conformal radiotherapy. 15, 16

BEV beam's eye view. 15

CBCT Cone-Beam CT. 16

cc cubic centimeters. 2, 35, 42, 46, 47

CE Compton Effect. 13

CT Computed Tomography. 1, 5, 11, 15, 16, 19, 25, 26, 29, 30

DRE Digital Rectal Exam. 10

DVH Dose-volume histogram. 1, 15, 22, 30, 34, 35, 40, 42, 47

EBRT External Beam Radiation Therapy. 11

HU Hounsfield Unit. 25, 26, 28

IGRT Image-Guided Radiation Therapy. 5, 11, 16

IMRT Intensity Modulated Radiotherapy. 5, 11, 15, 16, 18

IVDT Image value-to-density table. 25, 27, 28, 29

kVCT kiloVoltage CT. 28

MLC Multileaved Collimator. 17, 18, 19

MRI Magnetic Resonance Imaging. 16

MVCT MegaVoltage Computed Tomography. 1, 6, 17, 20, 24, 28, 29

OAR Organ At Risk. 5, 15, 19, 22, 29

PE Photoelectric Effect. 13

PSA Prostate-Specific Antigen. 10

PTV Planning Treatment Volume. 5, 15, 19, 22, 24, 47

ROI Region Of Interest. 19, 26, 29

SAD source to axis distance. 18

TD TomoDirect. 18

TH TomoHelical. 18, 19

TNM Tumour, Node, Metastasis. 10

TRUS Transrectal ultrasound. 10

Chapter 1. Introduction

1.1 Overview

Prostate cancer is a very common disease among men, ranking among the top five cancers for both incidence and mortality[15].

Surgery and Radiotherapy are the standard therapy choices for prostate cancer, Most of Prostate cancer patients that undergo a radiotherapy gets treated by Intensity Modulated Radiotherapy (IMRT), a technique used to optimize a given dose and protect Organ At Risk (OAR) and also Image-Guided Radiation Therapy (IGRT) which uses CT images to accurately adjust patient position and precisely target the tumor.
Prior to the treatment, An image registration[1] is taken to ensure that OARs (Bladder, Rectum ...) and Planning Treatment Volume (PTV) have a relatively identical shape, volume to the treatment plan to avoid certain complexities. To guarantee reproducibility of the treatment setup, the patient is educated and demanded to go through a preparation procedure. Some centers may instruct the patient to empty the bladder and drink a specified amount of water, insert spacers, take pharmaceuticals to empty rectum, may be required to go through surgical procedure or follow dietary instructions such as fasting to avoid gas and bloating.

Patient preparation of the bladder and rectum is done to reduce the motion and variability of the prostate and prostate bed, although it may be a challenge to maintain a consistent variation as it depends on the patient dedication to the instructions, patient's metabolism, unrelated side diseases and other factors.

1.2 Objectives

The primary goal of this study is to **validate the efficacity of the preparation protocol by analyzing bladder variation in radiotherapy**. this procedure will be standardized to quantify the range of tolerance in bladder, allowing us to continue the treatment seamlessly without further steps to re-prepare the patient.

[1]Registration is the process of establishing spatial correspondences between images

Additionally, secondary objectives will include :

1. Investigating impact of poor preparations.
2. Evaluating the necessity of re-preparations when needed.

1.3 Limitations

Patient variability is one of the most considerable issues in this study as the patients anatomical and physiological differences may contribute to bladder filling variations, taking into account patient's adherence to prescribed preparation protocol affecting the results. furthermore, the sample size may impact the statistical power knowing that the study is conducted with minimal number of patients. moreover, the image quality of MVCT will be a hindrance while interpreting the image data necessitating a bias countouring.

Chapter 2. Literature review

2.1 Prostate Cancer

2.1.1 Prostate gland

The prostate is a gonad that lies in the middle of the pelvis beneath the urinary bladder and in front of the rectum. It surrounds the urethra and the ejaculatory ducts. The seminal vesicles are located just above the prostate. These two little glands secrete about 60% of the substances that make up the semen. The seminal vesicles connect with the ejaculatory ducts in the prostate. The nerves that control the erectile function run along the sides of the prostate. While undergoing therapy for prostate cancer, there is a substantial risk of damage of these nerves with erectile problems as a sequel[2].

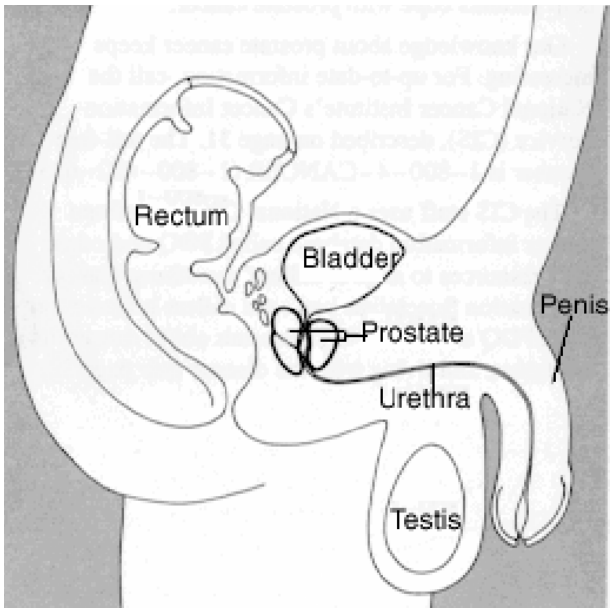

Figure 2.1: The figure shows the location of the prostate[2].

2.1.2 Epidemiology

Prostate cancer stands out as a significant health concern for men worldwide, ranking as the second most commonly diagnosed cancer and the fifth leading cause of cancer-related deaths among men in 2020 as can be seen in figure (2.2). Remarkably, prostate cancer is the most frequently

diagnosed cancer in men in more than half of the countries worldwide [17], underscoring the widespread impact and importance of addressing this disease on a global scale. Prostate cancer develops in the prostate and may metastasize to other parts of the body. It might cause pain and difficulties while urination such as; difficulties to start and maintain a steady stream of urine, frequent urination or increased urination at night. Other symptoms are; blood in the urine and erectile dysfunction, or problems during intercourse. However, since most tumors develop in the outer, rear part of the prostate, symptoms do not appear until the tumor has grown a bit[2].

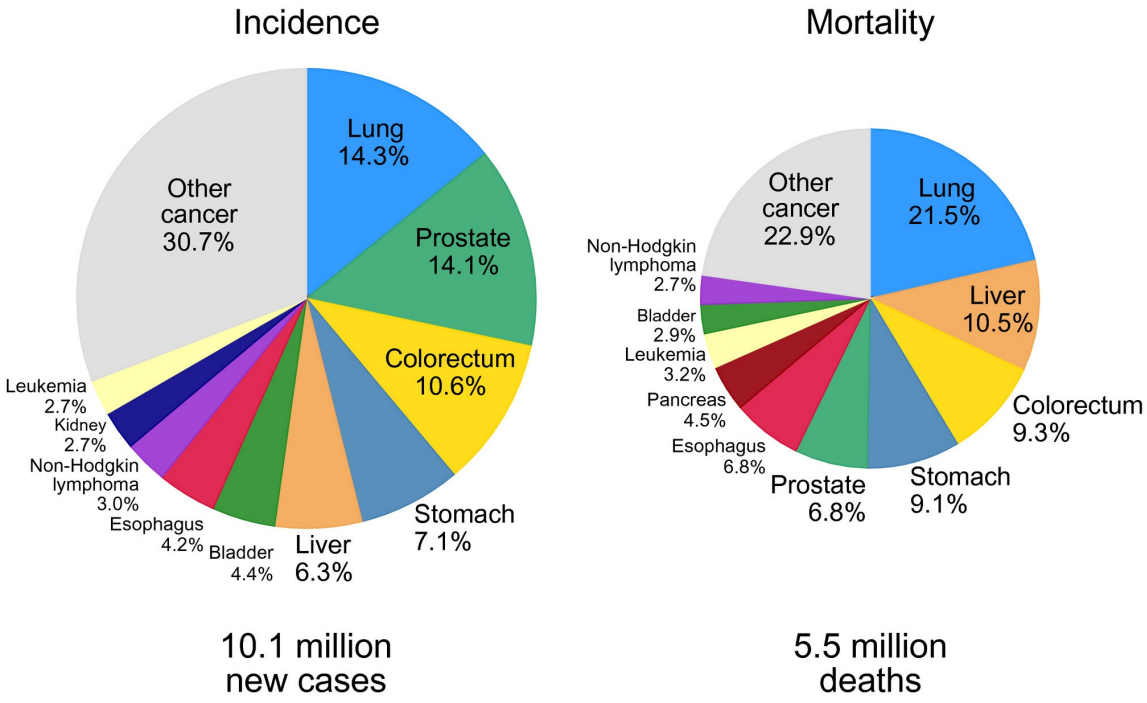

Figure 2.2: Global Distribution of Cases and Deaths for the Top 10 Most Common Cancers in 2020 for men

Prostate cancer remains a critical public health issue in Algeria, with data from the Global Cancer Observatory and the World Health Organization highlighting its significant impact on the population. In 2022, prostate cancer constituted approximately 9.1% of all new cancer cases in the country, with an estimated 2,421 new diagnoses. Furthermore, prostate cancer was responsible for about 4.2% of all cancer-related deaths in Algeria in 2022, accounting for roughly 1,115 deaths.

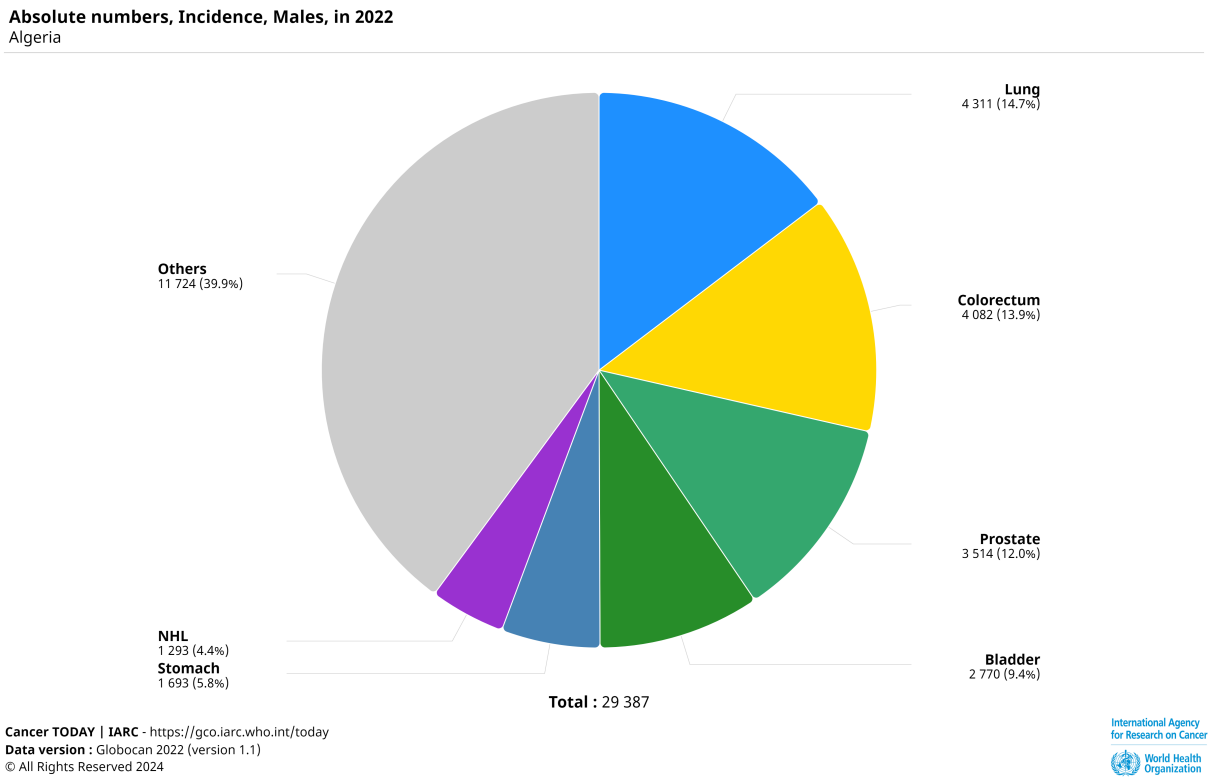

(a) Incidence

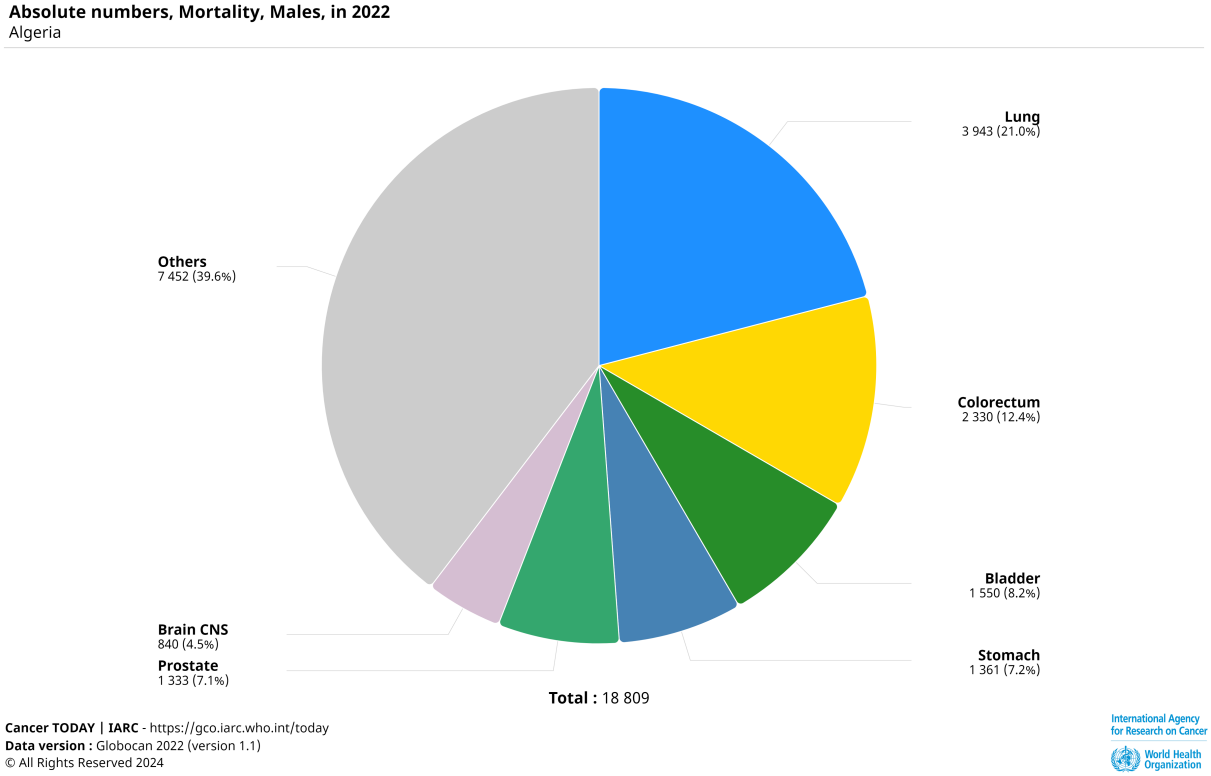

(b) Mortality

Figure 2.3: Distribution of prostate cancer incidence and mortality among males in Algeria

2.1.3 Types of prostate cancer

Prostate cancer primarily manifests as adenocarcinomas, comprising over 95% of cases. These adenocarcinomas originate in the gland cells of the prostate, responsible for producing prostate fluid, which mixes with sperm to form semen. The two main types of adenocarcinomas are acinar adenocarcinoma and ductal adenocarcinoma, with the latter being more aggressive and spreading faster. However, there are several rare forms of prostate cancer, collectively making up the remaining percentage. These include small-cell carcinoma, which is typically found in the lungs but can occur in the prostate and spreads rapidly; squamous cell carcinoma, more commonly a skin cancer, originating from flat cells covering the prostate; transitional cell (or urothelial) cancer, growing in the urethra and sometimes originating in the prostate before spreading; neuroendocrine tumors, arising from hormone-producing cells, occasionally developing within prostate cells; and soft tissue sarcoma, an extremely rare occurrence originating in supportive tissues within the prostate. Each of these rare types represents a small fraction of prostate cancer cases, with some being highly aggressive and prone to rapid spread[6].

2.1.4 Diagnosis and Staging

Prostate cancer diagnosis involves a combination of screening tests, clinical evaluation, and confirmatory procedures. Screening typically includes a Digital Rectal Exam (DRE) and a Prostate-Specific Antigen (PSA) blood test. PSA is produced in the prostate and is, as the name hints, specific for this gland. The PSA leaks out to a serum and prostate cancer makes the serum level rise. The level of the serum in the blood also gives a hint of the stage of the tumor. A patient with PSA <3mg/L has a low probability of cancer while <10 mg/L indicates a non-metastasized tumor[2]. Abnormal findings on these tests may prompt further evaluation with imaging studies like Transrectal ultrasound (TRUS) or prostate biopsy to confirm the presence of cancer[7]. Staging of prostate cancer is crucial for determining the extent of the disease and guiding treatment decisions. The Tumour, Node, Metastasis (TNM) staging system, which categorizes tumors based on their size and spread, along with PSA levels and Gleason scores, helps stratify patients into risk categories. The extent of the tumor (T) is classified from T1 to T4, with higher T values indicating more involvement of the prostate and surrounding structures. The node category is either no sample (X), no positive nodes (0), or (1) to indicating lymph node involvement. Metastatic disease is categorized as no spread (0) or (1) with three subcategories [7]. Risk categories such as very low risk and low risk are defined based on parameters like T stage, Gleason score, PSA levels, and biopsy core involvement. Treatment decisions are often guided by these risk categories, with options ranging from active surveillance for low-risk cases to more aggressive treatments like surgery, radiation therapy, hormone therapy, and chemotherapy for higher-risk disease. Individualized treatment plans take into account the patient's age, comorbidities, and disease characteristics, with the goal of maximizing outcomes while minimizing side effects[7].

2.1.5 Treatment

Prostate cancer treatment options include a range of modalities tailored to individual patient characteristics and disease stage. These options include External Beam Radiation Therapy (EBRT), Brachytherapy, Surgery, Active Surveillance, Chemotherapy, Cryotherapy[7]. EBRT, also known as radiotherapy, is a cornerstone in the management of prostate cancer. This treatment involves a series of daily sessions to precisely deliver radiation to the prostate, aiming to eradicate cancer cells effectively. Prior to initiating treatment, a comprehensive plan is developed by the radiation oncologist based on biopsy results, imaging studies, and physical examinations. This plan may involve a CT scan in the treatment position, sometimes with supportive devices to ensure consistent positioning during therapy. Additional measures like bladder filling or rectal protection gels may be employed to minimize side effects. Marker seeds may be placed in the prostate to enhance treatment accuracy. Utilizing advanced technologies like IMRT and IGRT, EBRT focuses radiation beams precisely on the prostate while sparing surrounding healthy tissues such as the bladder and rectum. These techniques optimize treatment efficacy while minimizing adverse effects. EBRT can be delivered through various approaches, typically in daily sessions over several weeks. Hypofractionated radiation, a condensed treatment regimen delivering slightly higher doses over a shorter period, has shown comparable outcomes to standard treatment durations.

2.2 Interaction photons matter

Radiation can be categorized as electromagnetic or particulate, photons are electromagnetic radiations that includes visible light, infrared and ultra violet, X rays and Gamma rays [1], each of them have a different range of wavelength and energy given by $E = h\nu = hc/\lambda$ where (c) is speed of light in vaccum and (λ) is the wavelength and (ν) is the frequency of the wave. Radiation can also be classified as non-ionizing or ionizing[1] radiation either directly or in-directly [1]. The interaction of photons with matter is a probalistic model known as cross-section, the resulting effect depends on the energy of the photon and the atomic number (Z) of the target material.

2.2.1 Compton Scattering

In Compton scattering, the incoming photon is deflected through an angle θ with respect to its original direction. The photon transfers a portion of its energy to the electron, which is then known as a recoil electron. Because all angles of scattering are possible, the energy transferred to the electron can vary from zero to a large fraction of the gamma-ray energy[11].

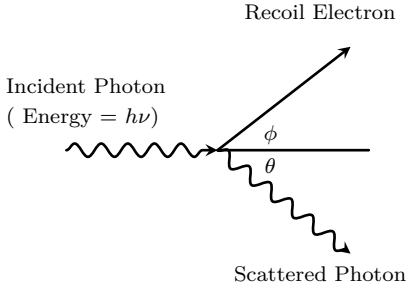

Using symbols from figure above and the conservation of momentum and energy we can deduce the energy of the diffused photon :

$$h\nu' = \frac{h\nu}{1 + \alpha(1 - \cos(\theta)} \tag{2.1}$$

Where $\alpha = \frac{h\nu}{m_0 c\check{s}}$. We can deduce from that the energy of the scattered photon at a angle zero $h\nu \approx h\nu'$ and the maximum value at angle of $\theta = 180°$ which corresponds to the backscatter event :

$$h\nu' = \frac{h\nu}{1 + 2\alpha} \tag{2.2}$$

2.2.2 Photoelectric effect

In the photoelectric absorption process, a photon undergoes an interaction with an absorber atom in which the photon completely disappears. In its place, an energetic photoelectron is ejected by

[1]The ability to remove an electron from it's orbit also known as ionizing poteniel.

the atom from one of its bound shells. The interaction with the atom as a whole and cannot take place with free electrons. For gamma rays of sufficient energy, the most probable origin of the photoelectron is the most tightly bound or K shell of the atom [11]. The photoelectron appears with an energy given by :

$$Te^{-} = h\nu - E_L \tag{2.3}$$

Where E_L is the binding energy of the photoelectron which is the majority of the photon energy.

2.2.3 The relative importance of types of interaction at 6 MeV

Between the two interactions (Compton Effect (CE) and Photoelectric Effect (PE)) at high energies (6 MeV), CE is the most dominant effect with a low atomic number Z of the absorber material (Carbon, Air, Water, Tissue, ...).However, PE becomes prevalent with high atomic number Z. See figure (2.4)

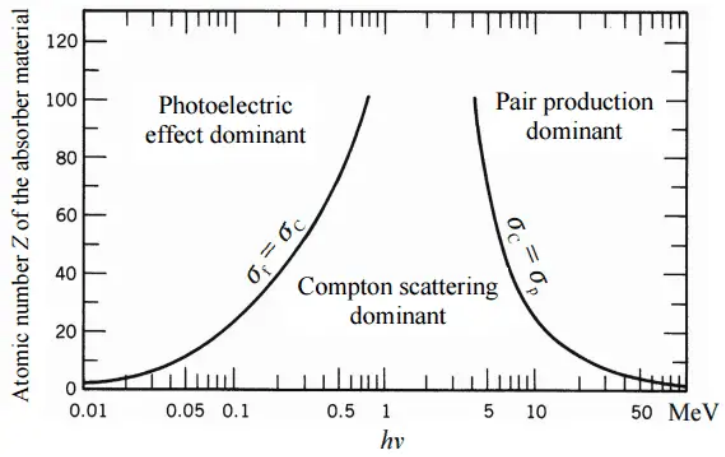

Figure 2.4: The relative importance of the three major types of gamma-ray interaction [11]

2.2.4 Attenuation of photons within materials

If we suppose a collimated monoenergetic photon beam striking an absorber of variable thickness x with an intial intensity I_0, the resulting transmitted beam will have an exponentiel intensity of I, with every photon that interacted with the absorber material is removed we conclude :

$$I = I_0 e^{-N\sigma_t x} \tag{2.4}$$

where :

$\sigma_t = \sigma_{cp} + \sigma_{pe}$

σ_{cp} Cross-section Compton

σ_{pe} Cross-section Photoelectric

N Atomic density (Atom per cm^3)

2.3 Radiotherapy

The first x-ray therapy began less than two months after the the x-ray discovery by Roentgen. Very little was known about the properties of these new rays. A major advance in the radiation field came in the late 1920s, a truly scientific approach of radiation therapy started where the amount of radiation to the patient was reported, compared, and used clinically. In the late 1930s, it was possible to treat tumors with multiple fields, crossfiring on the tumor in order to achieve a higher dose at the tumor, while spreading the dose out over normal tissues. Infact, the first radiotherapy treatment performed by Grubbe actually included the use of lead sheet to protect the healthy tissues aronud the lesion. However, the ability to quantitatively analyze the relationship between complications, dose, and volume of tissue irradiated was not available until the 1980s, after the CT scanner and 3-D treatment planning were developed[8].

2.3.1 Intensity-modulated radiation therapy

The introduction of CT into radiation oncology in the 1980s enabled treatment planning based on three-dimensional anatomical information of the tumor and surrounding healthy tissues, thus facilitating the establishment of threedimensional conformal radiotherapy (3D-CRT). The key features of 3D-CRT treatment planning include beam's eye view (BEV) design of treatment fields and plan evaluation. BEV allowed for finding a beam direction that could irradiate the tumor without the beam passing through nearby critical organs. DVHs and isodose distributions became essential tools for plan evaluation. Together with the progress in threedimensional (3D) image processing, the 3D volume information from CT also enabled accurate dose calculation using the convolution-superposition method, allowing the inhomogeneous distribution of tissues to be more accurately handled. Whereas 3D-CRT exploits field shape conformation to improve target dose conformality, the OARs located in the groove region of a concave target volumes cannot be saved from the target dose, as shown in figure (2.5). In conventional 3D-CRT, the irradiation field shape coincides with the shape of the target according to the incidence direction of the irradiation beam, while in IMRT, the beam intensity is modulated according to the arrangement of the target and surrounding organs. The intensities of the rays that pass through OARs are reduced, while the intensities of the rays go primarily through the target volume are increased. The inhomogeneity caused by the 'intentionally non-uniform intensity' of a beam is compensated for by beams from other directions. Physically, a feature of the IMRT technique is to enhance control over the 3D dose distribution through the superposition of a large number of independent segmented fields, either from a number of fixed directions or from directions distributed on one or more arcs. By this method of adding intensity modulation to geometric shaping, the IMRT dose distribution can be rendered concave, as opposed to the convex-shaped coverage accomplished with 3D-CRT, where geometric conformal shaping of a uniform intensity beam is performed. Therefore, IMRT can enable dose reduction to OARs located within a concave area of the PTV[5].

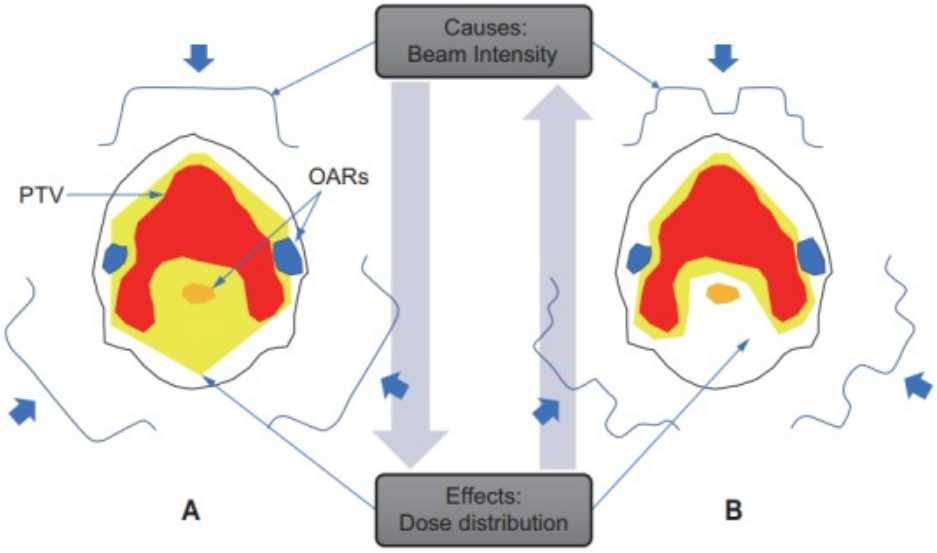

Figure 2.5: Comparison of the principle of 3D-CRT (A) and IMRT (B) with illustrations of forward vs. inverse planning. [5]

2.3.2 Image-guided radiation therapy

IGRT is a cutting-edge approach in radiation oncology that leverages advanced imaging technology to refine the precision and accuracy of cancer treatments. The primary objective of IGRT is to reduce uncertainties in target positioning during radiation therapy by integrating real-time imaging techniques. IGRT is a technique that addresses two primary types of organ movements that can impact the effectiveness of radiotherapy: intra-fraction organ motion and inter-fraction organ movement. inter-fraction organ movement involves changes in organ position or shape that occur between different treatment sessions. Pre-treatment imaging is used to tackle this issue in IGRT. Detailed images of the tumor and surrounding tissues are acquired before each radiation therapy session, typically utilizing techniques such as (CT scans, Magnetic Resonance Imaging (MRI), Ultrasound imaging, ... etc.) to ensure accurate targeting of the tumor area despite these changes. On the other hand, Intra-fraction organ motion refers to the changes in the position of organs during a single treatment session. IGRT addresses this through real-time imaging during treatment delivery. This allows for continuous monitoring of the tumor position and adjustment of the radiation beam in response to any movements, which is particularly beneficial in therapies targeting mobile organs such as those in lung cancer treatment. The techniques usually used in real-time imaging are: On-Board imaging systems, 4D CT, Cone-Beam CT (CBCT)[18].

By addressing both intra-fraction and inter-fraction movements, IGRT aids in minimizing the margins involved in defining the target volume, thereby safeguarding healthy tissues from unnecessary radiation exposure. The advantages of IGRT encompass improved treatment outcomes, enhanced tumor control rates, reduced side effects, and the potential for dose escalation to optimize therapeutic efficacy while minimizing toxicity.

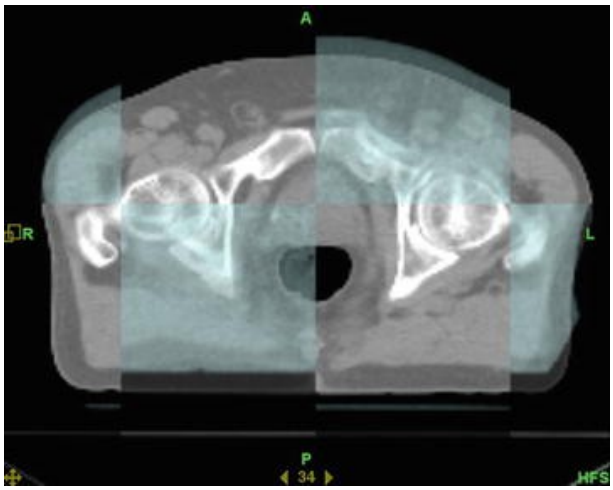

Figure 2.6: Patient setup verification using MVCT image guidance.

2.3.3 Tomotherapy

"Tomotherapy", which literally means "slice therapy", is a term derived from tomography. The basic idea is to put a linear accelerator or other radiation-emitting device into a CT-like ring gantry configuration and deliver therapeutic radiation using a rotating fan beam which is modulated by a binary Multileaved Collimator (MLC) system, while the patient moves through the gantry in the longitudinal direction. The system would use a MVCT for treatment verification[13].

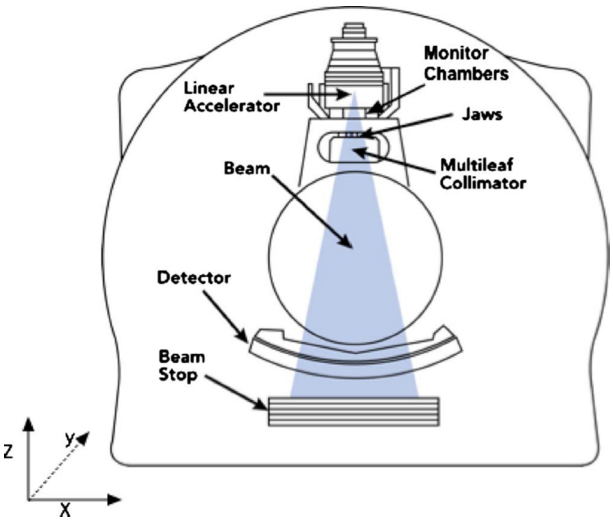

Figure 2.7: Diagram of of the main components TomoTherapy unit.

TomoTherapy Hi-Art was first developed at the University of Wisconsin, Madison, WI, USA. The TomoTherapy beam is generated by a 6 MV linear accelerator that is mounted on a slip ring gantry. The beam passes through a primary collimator and is further collimated into a fan-beam shape by an adjustable jaw. For further collimation, a binary MLC system is used. The ring gantry also contains a detector system that is mounted opposite the accelerator and is used to collect data for MVCT acquisition. A beam stopper is used to reduce room-shielding

requirements. Figure 2.7 shows the general layout of the tomotherapy unit. Contrary to other systems the source to axis distance (SAD) is 85 cm instead of the usual 100 cm[10, 12].

The radiation field has a fan shape with an extension of 40 cm in the lateral (x) direction at isocenter. In the superior-inferior, or y-direction, where the beam is also collimated by an adjustable jaw (secondary collimator) opening. In principle, this y-jaw can collimate the beam to any size that is smaller or equal to 5 cm but typically, only three distinct treatment slice widths are commissioned in the treatment planning system for clinical use. These fields have an extension of 1.0, 2.5, and 5.0 cm at isocenter in the y-direction. A binary 64 leaf collimator is used to divide the fan beam in the x-direction. The MLC leaves travel in the y-direction as indicated in figure (2.8). Each MLC leaf is either closed or open and intensity modulation is achieved via leaf specific opening times. The MLC is pneumatically driven. Because the tomotherapy system is a dedicated IMRT system it differs in several ways from other radiotherapy systems. The most important difference are the absence of a flattening filter, a thin target, an electron stopper, a beam hardener and a compact primary collimator, which cause the radiation field to be significantly different from that of other treatment units[10, 12].

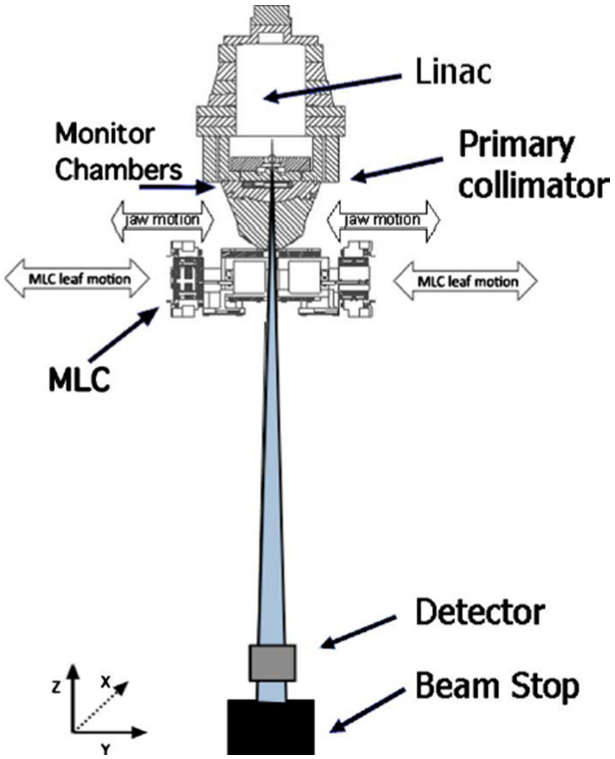

Figure 2.8: Lateral view of the beam collimation components..

TomoTherapy also offers two delivery techniques, Helical Tomotherapy also known as TomoHelical (TH), is a technique where the radiation is delivered to a patient in a helical way, obtained by concurrent gantry rotation and couch/patient travel[10].The other technique is a new system upgrade named TomoDirect™ was introduced to increase the versatility of the tomotherapy platform. TomoDirect (TD) is a nonrotational treatment option implemented on the TomoTherapy Hi-Art system that allows user to plan and deliver radiation treatments using coplanar static

beams, with the couch moving at a constant speed through a fixed binary MLC that modulates the beam. After the patient has been treated with one gantry angle, the gantry is rotated to a different angle and the patient is again passed through the bore for the delivery of the subsequent field[4, 9].

2.3.4 Radiotherapy workflow

Simulation

A prostate cancer radiotherapy conventionally is planned with a full bladder to result in a better sparing of bladder and small bowel. Generally, the patient is instructed to void bladder and drink a specific amount of water and to empty rectum using a prescribed pharmaceutical. The patient will be also recommended to take a walk around the center to accelerate bladder filling. Then, A wedge, foam shells, couch pillow will be chosen for the patient depending on his height and width. Right after that, he is put on the couch with a specified arms positions with metallic (Lead) beads fixed onto him at a slice zero (isocenter of the patient) as a reference to the prostate and a picture will be taken to the beads positions. The radiology technician will fill the patient's data right before the CT scan including patient's full name, age, disease and picture and also fill a form (Restraint table) describing arms positions, wedge, used pillow ... After that, The technician starts the acquisition and have a doctor approve the scan and the beads are removed from the patient and replaced with tattoos.

Target Contour

Radiation therapists carefully contour necessary target volumes (PTVs), which includes the tumor and any nearby lymph nodes at risk of containing cancer cells. They also identify critical structures and OARs, such as the bladder, rectum, and bowel.

Treatment Planning and Optimization

Using the TH treatment planning system, physicist develop a treatment plan tailored to the individual patient. This involves determining the optimal radiation dose, leaf modulation and used Region Of Interests (ROIs). The treatment plan undergoes iterative optimization to ensure that it meets the dose constraints for both the target volume (PTV) and critical structures (OARs). After a certain number of iterations, the penalties are adjusted interactively to "push" or modify the dose patterns, adjusting the parameters, and then continue. The decision to make the change can be deduced from the isodose pattern, which is updated regularly on the screen. After a certain number of iterations, the isodose pattern plateaus, indicating that the dose algorithm calculation reaches a cost minimum or near a minimum. The process is repeated until an acceptable plan is obtained. The acceptability of the treatment plan is evaluated to ensure that the plan meets the target conformity requirements and normal tissue dose-volume constraints[16].

Quality Assurance

The delivery quality assurance is an essential component of the dose delivery systems. It involves the measurements of the patient treatment fluence directed at a phantom and compared against the dose distribution generated by the treatment planning. The dose planes can be exported to the vendor's software for isodose distribution comparison with the measurements. In addition, an absolute point dose measurement in the "Cheese" or delivery quality assurance TomoPhantom can also be taken[16].

Treatment Delivery

Before each tomotherapy session, the patient prepares their bladder as prescribed by the physician. While the patient is lying on a specialized treatment couch that moves through a ring-shaped gantry, the technician initiates the MVCT scan to assess whether the bladder requires further preparation to avoid potential complications.

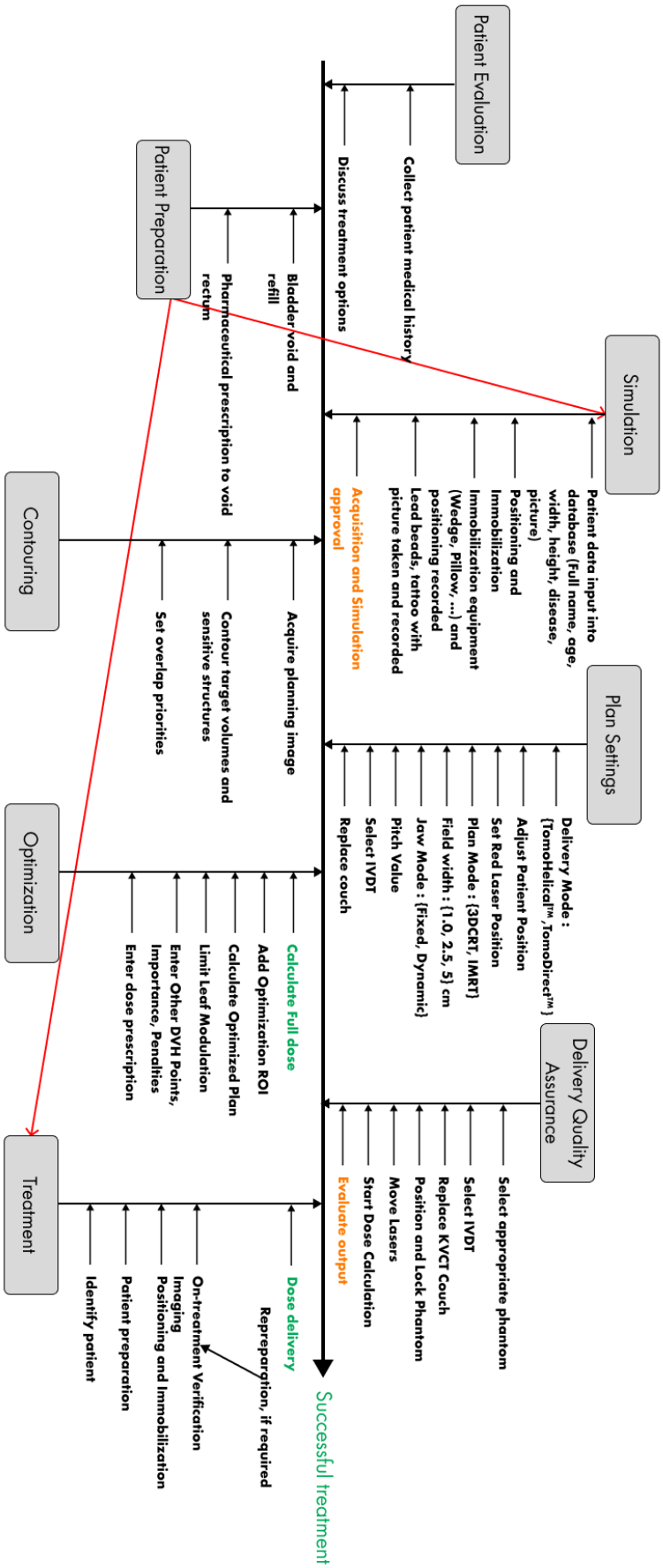

Figure 2.9: Tomotherapy treatment process tree

2.3.5 Dose Volume Histogram

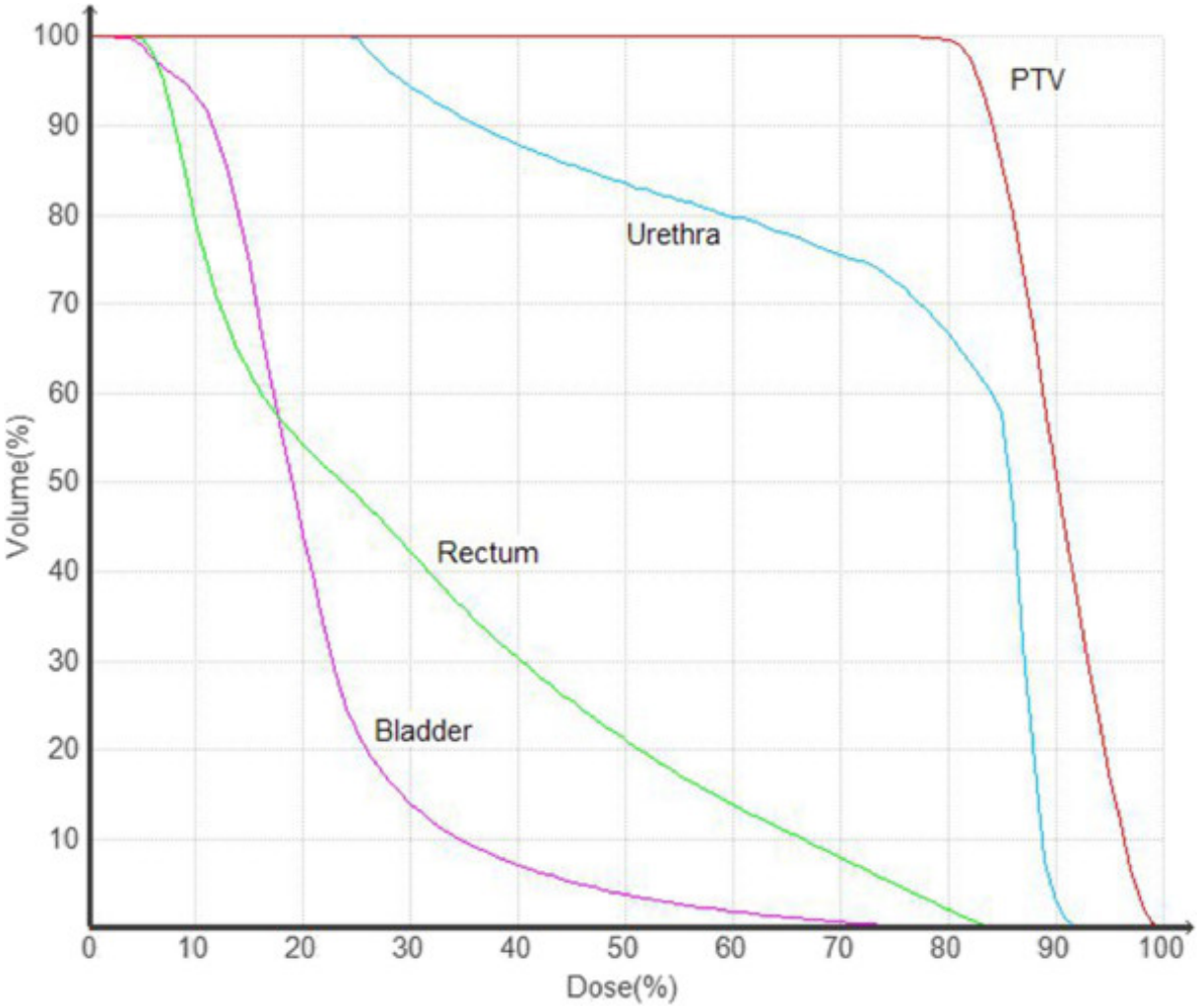

Figure 2.10: Typical DVH for the target volume PTV and healthy OARs[3].

A DVH is the common approach for summarizing the three-dimensional dose-volume data. A DVH is generated by tallying the doses delivered to each voxel of tissue and representing that information as a cumulative histogram of dose (x-axis) and volume (y-axis). Each point along the histogram (V_x) represents the volume of that organ (generally, a percentage) receiving an amount that is more than or equal to a certain dose (For example, V_{20} is the volume of an organ receiving at least 20 Gy). A DVH can be readily visualized and provides a quick and easy way to describe the dose-volume characteristics of the three-dimensional dose distribution. However, a DVH achieves this by discarding all spatial information. Functional and structural complexities and spatial variations in function and sensitivity are thus not considered in DVHs. Possible interactions between organs are also not considered with this construct. The critical metrics that will be considered in this review are the mean organ dose and discrete points on the DVH. The term D_x reflects the minimum dose to the "hottest" x% (generally, percentage of total volume) of tissue [14].

Chapter 3. Materials and methodologies

3.1 Materials description

The study consisted of two study cases. The first study case included 10 randomly selected patients who received hypofractionated prostate tomotherapy were used to compute dose volumes for each fraction, their treatment plan were performed by experienced physicists using TomoTherapy planning system. Contours and dose computation of bladder volume of each fraction were done by medical physicists students with a supervision of an experienced physicist using RaySearch RayStation™and Planned Adaptive™. The second study case included 24 unique patients that have been randomly surveyed on their treatment preparation.

Figure 3.1: Accuray TomoTherapy machine used for the study at SIDI Abellah ONCOLOGY CENTER

3.1.1 Dose constraints and objectives

Hypofractionated prostate treatments were planned with 95% of PTV volume recieving atleast 95% of the prescribed dose ($V_{95\%} > 57Gy$), where the prescribed dose is 60 Gy in 20 fractions (3Gy per fraction). See table 3.1 below.

Organe	Constraint
Bladder	$V_{40.8} < 50\%$
	$V_{48.6} < 25\%$
	$V_{60} < 5\%$

Table 3.1: Bladder dose constraints adapted by the center in a hypofractionated treatment

3.2 Patient preparation

Before simulation and prior to every treatment session, All surveyed patients were instructed to void their bladder and rectum using a prescribed pharmaceutical. Patients were recommended to drink two small water bottles (2 x 500 ml) atleast one hour before the treatment. Patients may be asked to re-prepare if a noticeable difference in bladder volume was seen by technicians using the MVCT. Patients were surveyed post-preparation regarding their water intake and drinking schedule (See figure 3.2).

Patient hydration survey

Questions
Q1 : How much did you drink today ?
Q2 : At what time did you drink them ?
Q3 : How many times did you go to the toilet today ?
Q4 : At what time did you go to the toilet?

ID	Age	Fraction	Q1	Q2	Q3	Q4

1

Figure 3.2: Survey form used for gathering information about patient's preparation

3.3 Dose calculation

3.3.1 IVDT

Image value-to-density table (IVDT) is a lookup table used to map CT images pixels values expressed in Hounsfield Unit (HU) to density values, It is used to calculate planning and verification doses. A **Cheese phantom** (also known as Virtual Water™phantom) was used to calculate it, which is usually utilized for calibration. the cheese phantom's large and small plugs are removed and the recommended plugs in the form (See figure 3.3) are put in a repartition as instructed (

See figure 3.4).

Figure 3.3: Used plugs in the acquisition

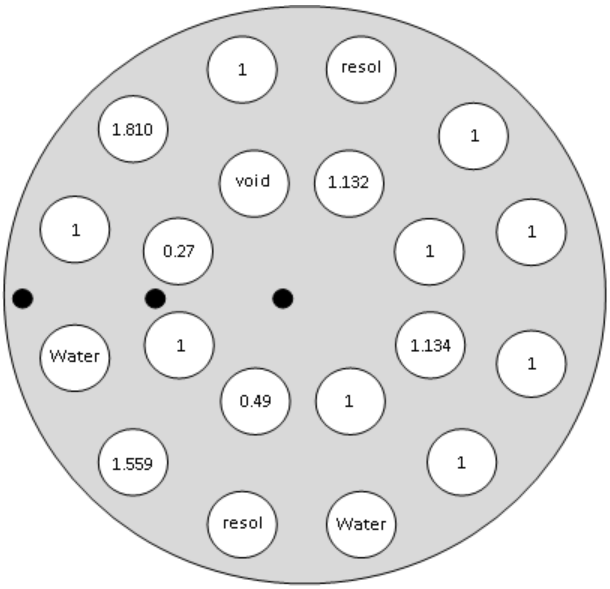

Figure 3.4: Repartition of cheese phantom density plugs

The used phantom is placed on the couch and directed towards the tomotherpy machine and aligned with the aid of green lasers. In the control unit, Acquisition parameters are adjusted such as acquisition pitch. Subsequently, slices in the slice selector are selected and with the button "Prepare scan" the software starts calculating couch position and rotation. Finally, the acquisition process is initiated by following the system's instructions.

CT images acquired were sent to another station with HU values extracted from the density plugs to be processed. The measurements were performed utilizing IQWorks version 0.7.2 and ImageJ version 1.54g, using a straightforward ROI selection and measurement approach (See figure 3.5).

Following the measurement, the obtained Image value-to-density table (IVDT) values are added to Image Value-to-density Calibration Table Editor in the planning system (See figure 3.6).

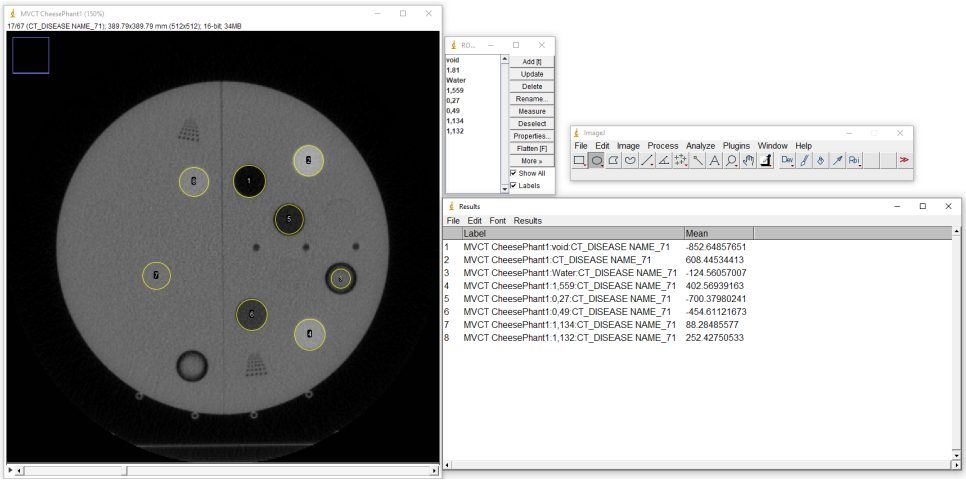

Figure 3.5: IVDT measurement using ImageJ

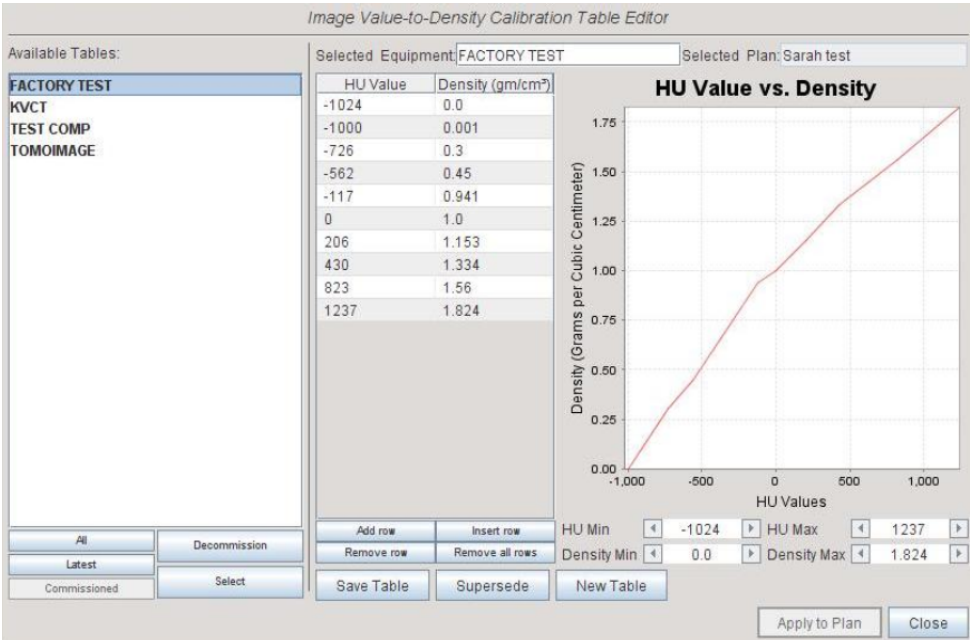

Figure 3.6: TomoTherapy™Planning Software IVDT Editor

Density Values (g/cm^3)	HU Value		
	TOMO1	TOMO2	TOMO3
1.81	627.90	675.27	543.21
1.559	425.31	465.96	391.95
1.134	88.93	107.92	78.97
1.132	256.4	279.82	218.65
1	-79.51	15.26	-116.95
0.49	-478.72	-491.36	-642.36
0.27	-703.61	-700.23	/
0	-1024	-1024	-1024

Table 3.2: Measured and used IVDT for each tomotherapy machine.

For TOMO2 (Tomotherapy Machine N°2), mean values from three different acquisitions with varying acquisition pitches were used. IQWorks was utilized to measure the values for TOMO1, and ImageJ was used for the rest. (See table 3.2)

3.3.2 Contouring and Segmentation

Figure 3.7: Image registration procedure between kVCT and MVCT scan images in RayStation™

Contouring the bladder for each fraction was an essential part of the second study case, where 10 patients underwent at least 20 MVCT scans. This resulted in a total of atleast 200 bladder

contours which included the contour of the bladder in the simulation CT, in the treatment session MVCT and after the patient re-preparation if required. CT Images from each acquisition in treatment sessions were imported to patient case and were registered with the planning CT. The MVCT image registration performed better with "Focus on bone structures" feature although minor manual adjustments were sometimes necessary following the process. In the structures definition tab, The window layout was changed to split and planning CT was set as a primary and the treatments CT images were set as secondaries. A new ROI was created as an OAR and delineated using the brush, boolean operations and interpolation.

The contours were exported in the patient data management tab to Planned Adaptive™(Hi-Art) by selecting RT structure file where the segmentations were done.

3.3.3 Verification and Summation dose calculation

Calculating a verification dose in the Planned Adaptive™in the Compute Dose tab (See figure 3.8) involved loading the appropriate image, structure (Contour) and IVDT for the tomotherapy machine the CT image was acquired on. A manual image registration may be required if instructed to. The merged image was created by saving the image and finally the verification dose can be calculated individually or in a batch.

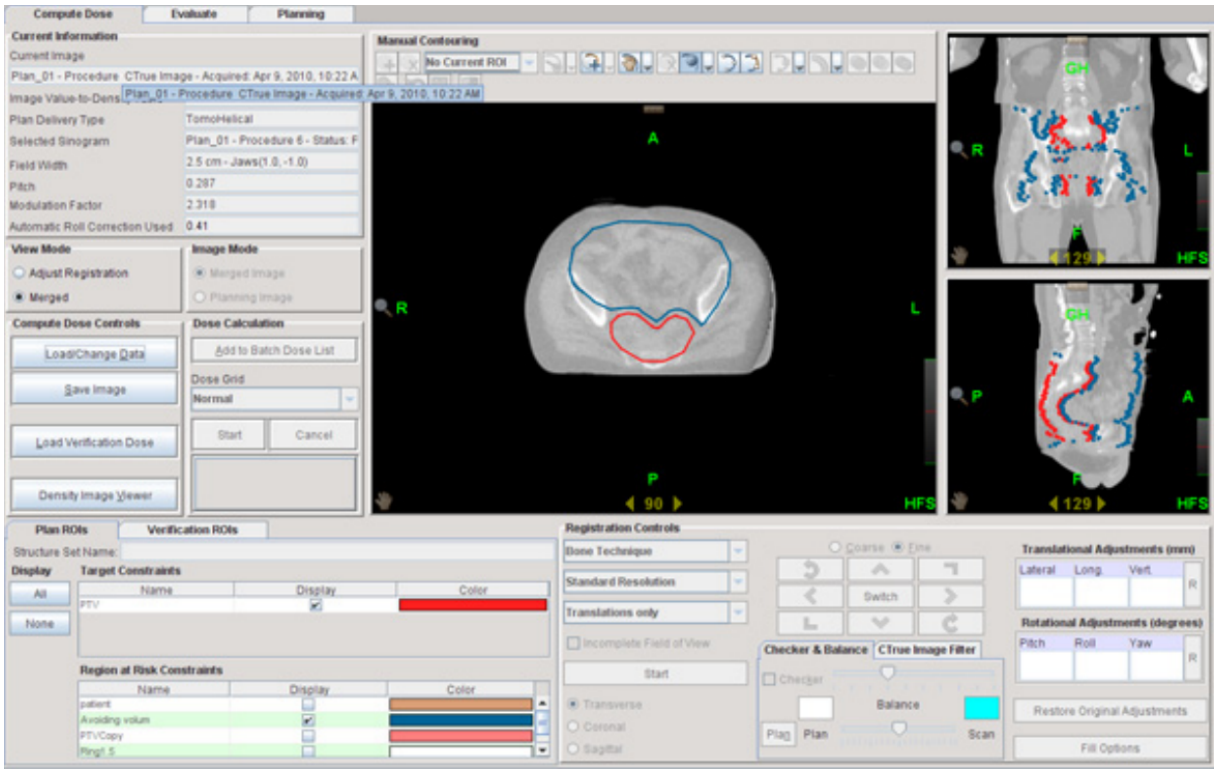

Figure 3.8: Planned Adaptive, Compute dose tab

After calculating verification doses for all fractions for a given patient, A summation dose was computed in the Planning tab by selecting the series of verification doses. All the verification doses were assessed when the summation dose finished loading in the Evaluate tab. This evaluation

included viewing and exporting the verification dose volume, planning dose volume, and the differences between verification dose and planning dose volumes. DVHs were evaulated either cumulatively or differentially with relative volume or absolute volume values.

All the summation doses, planning doses, CT images, contours were exported for further analysis.

3.4 Dose-volume variation analysis

The majority of subsequent work was conducted using Python within the Windows Subsystem for Linux environment, leveraging PlatiPy — an image processing and analysis toolkit library. The exported data from Planned Adaptive™such as summation doses, planning doses, and contour files of each patient were loaded and analyzed. These datasets were used in computing bladder volumes along with associated metrics, constructing DVHs, and establishing dose volume constraints for comparative analysis. Furthermore, the research encompassed performing simple regression analyses to delineate correlations among various parameters.

Chapter 4. Results

4.1 First study case : Dose-volume variation analysis

4.1.1 Inter-fraction DVH Comparison

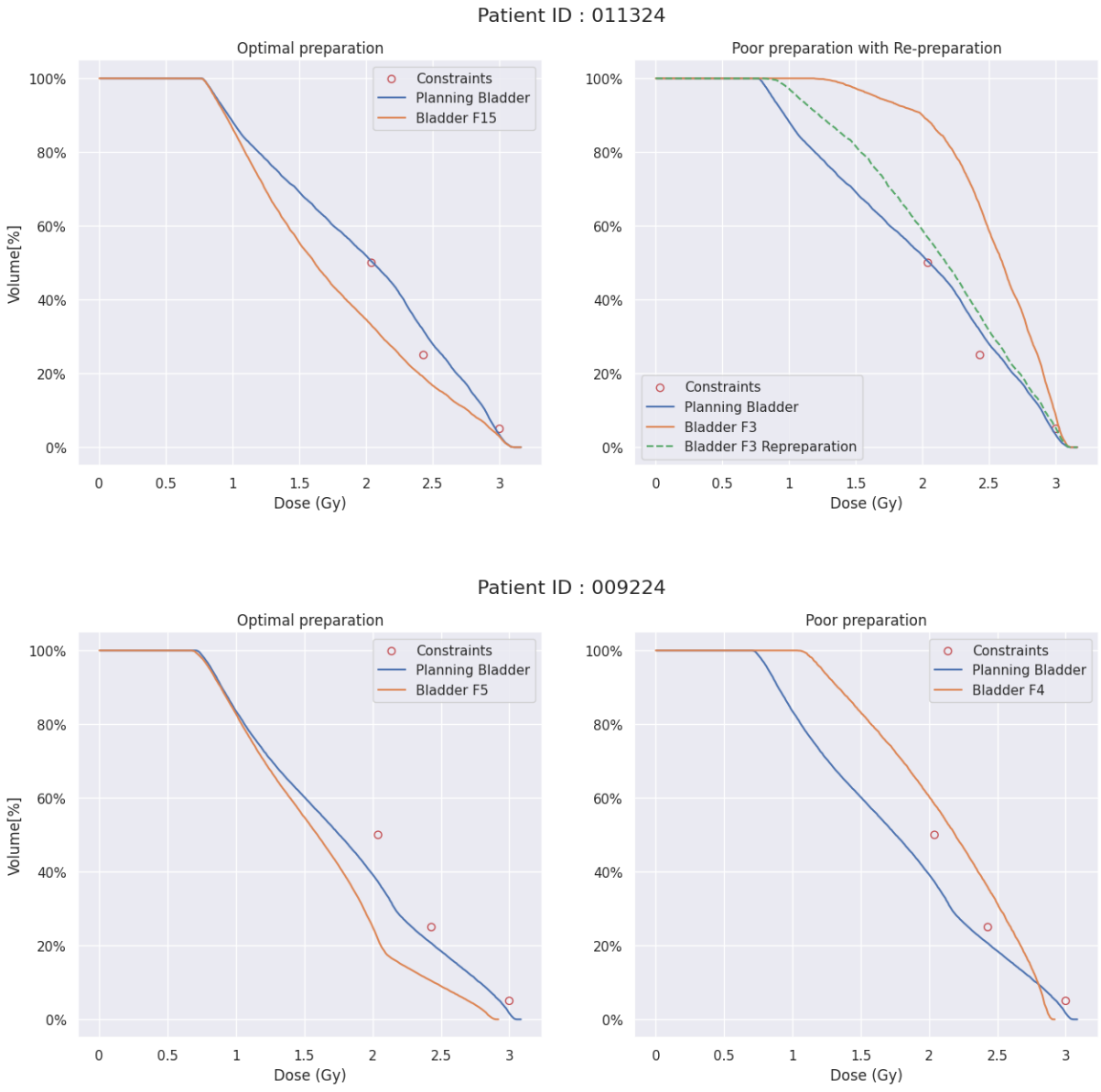

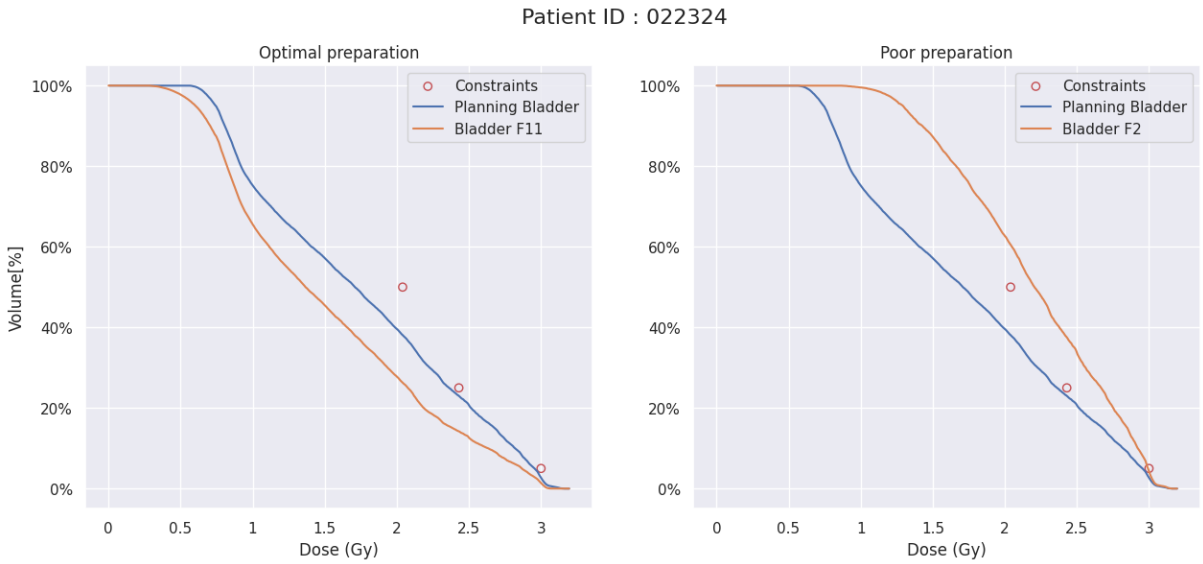
Patient ID : 022324
Optimal preparation
Constraints
Planning Bladder
Bladder F11
Poor preparation
Constraints
Planning Bladder
Bladder F2
Volume[%]
Dose (Gy)

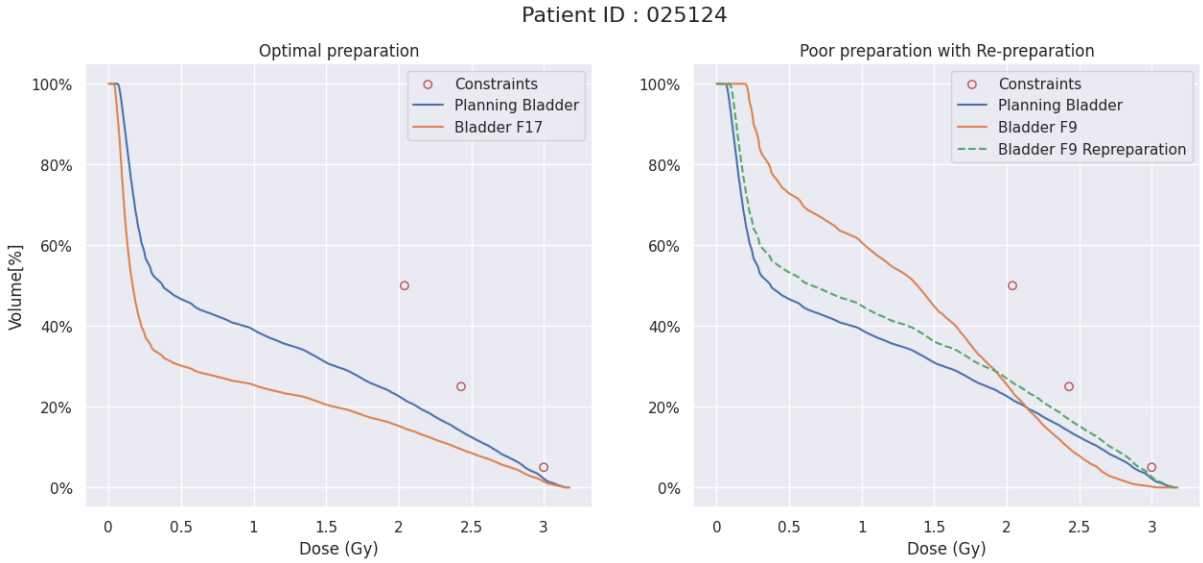
Patient ID : 025124
Optimal preparation
Constraints
Planning Bladder
Bladder F17
Poor preparation with Re-preparation
Constraints
Planning Bladder
Bladder F9
Bladder F9 Repreparation
Volume[%]
Dose (Gy)

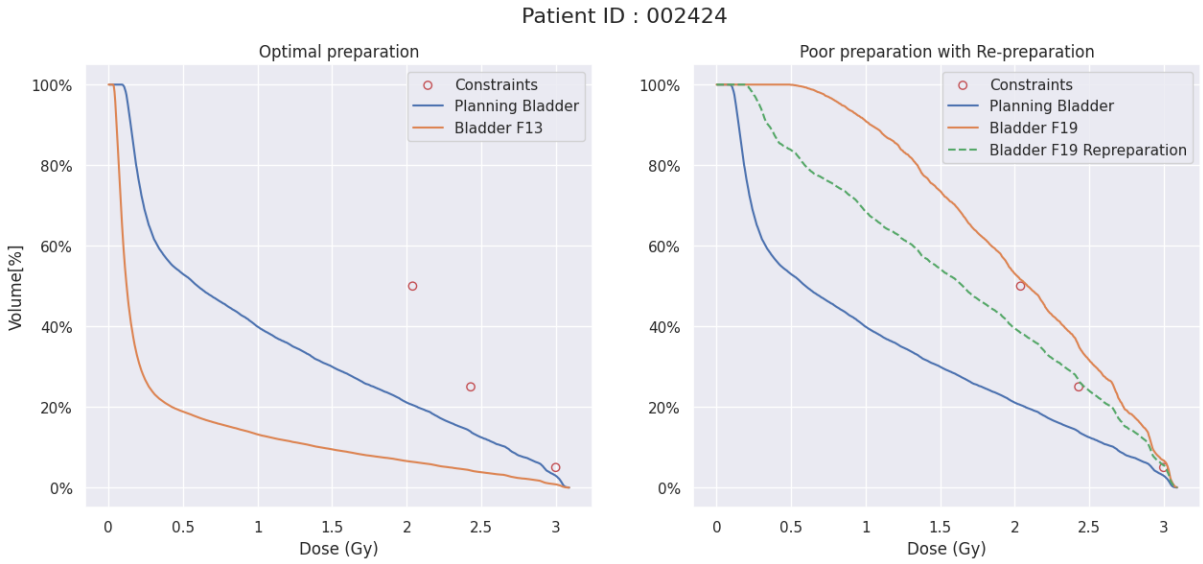
Patient ID : 002424
Optimal preparation
Constraints
Planning Bladder
Bladder F13
Poor preparation with Re-preparation
Constraints
Planning Bladder
Bladder F19
Bladder F19 Repreparation
Volume[%]
Dose (Gy)

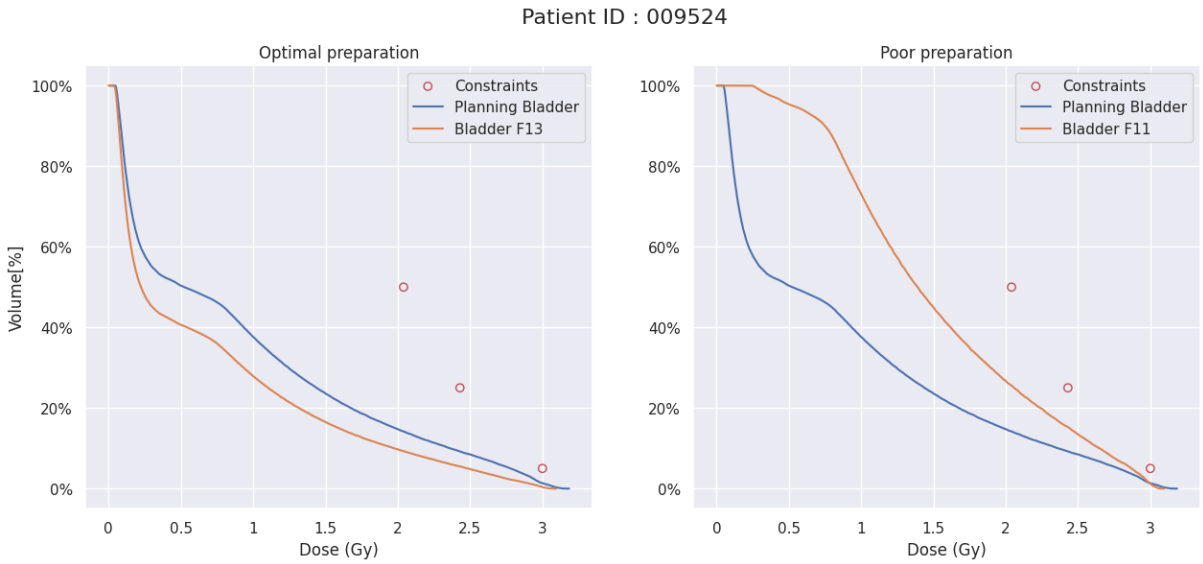
Patient ID : 009524
Optimal preparation
Poor preparation
Constraints
Planning Bladder
Bladder F13
Bladder F11
Volume[%]
Dose (Gy)

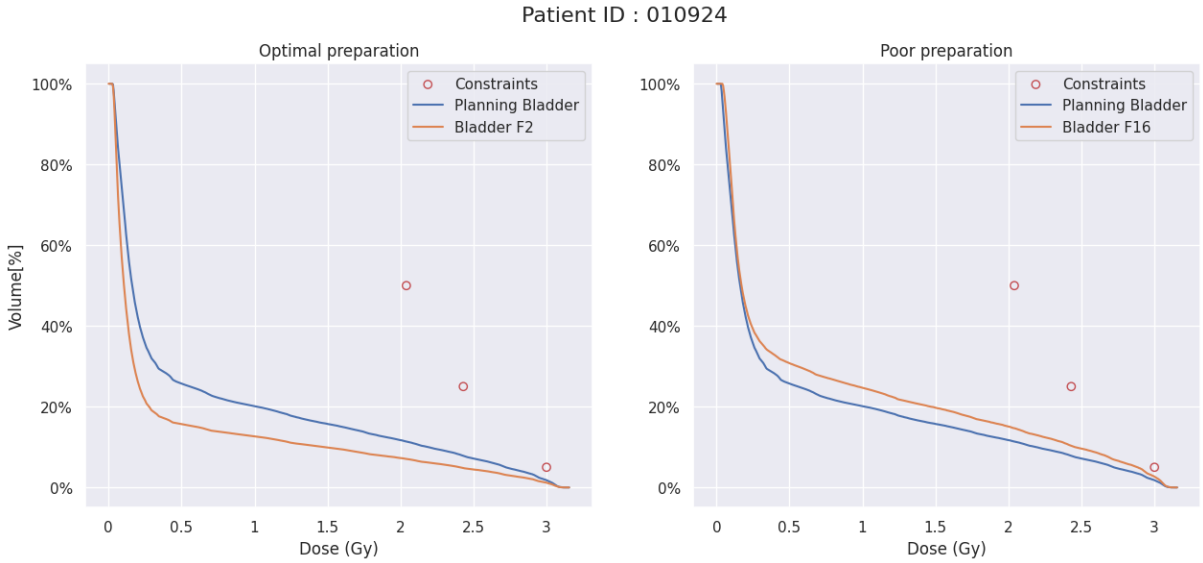
Patient ID : 010924
Optimal preparation
Poor preparation
Constraints
Planning Bladder
Bladder F2
Bladder F16
Volume[%]
Dose (Gy)

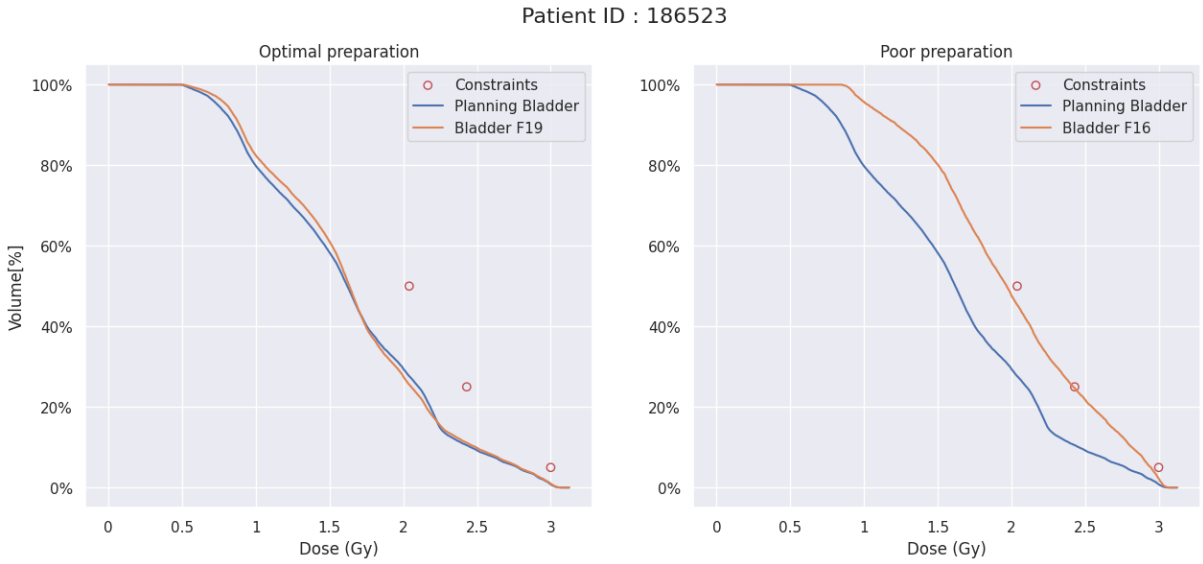
Patient ID : 186523
Optimal preparation
Poor preparation
Constraints
Planning Bladder
Bladder F19
Bladder F16
Volume[%]
Dose (Gy)

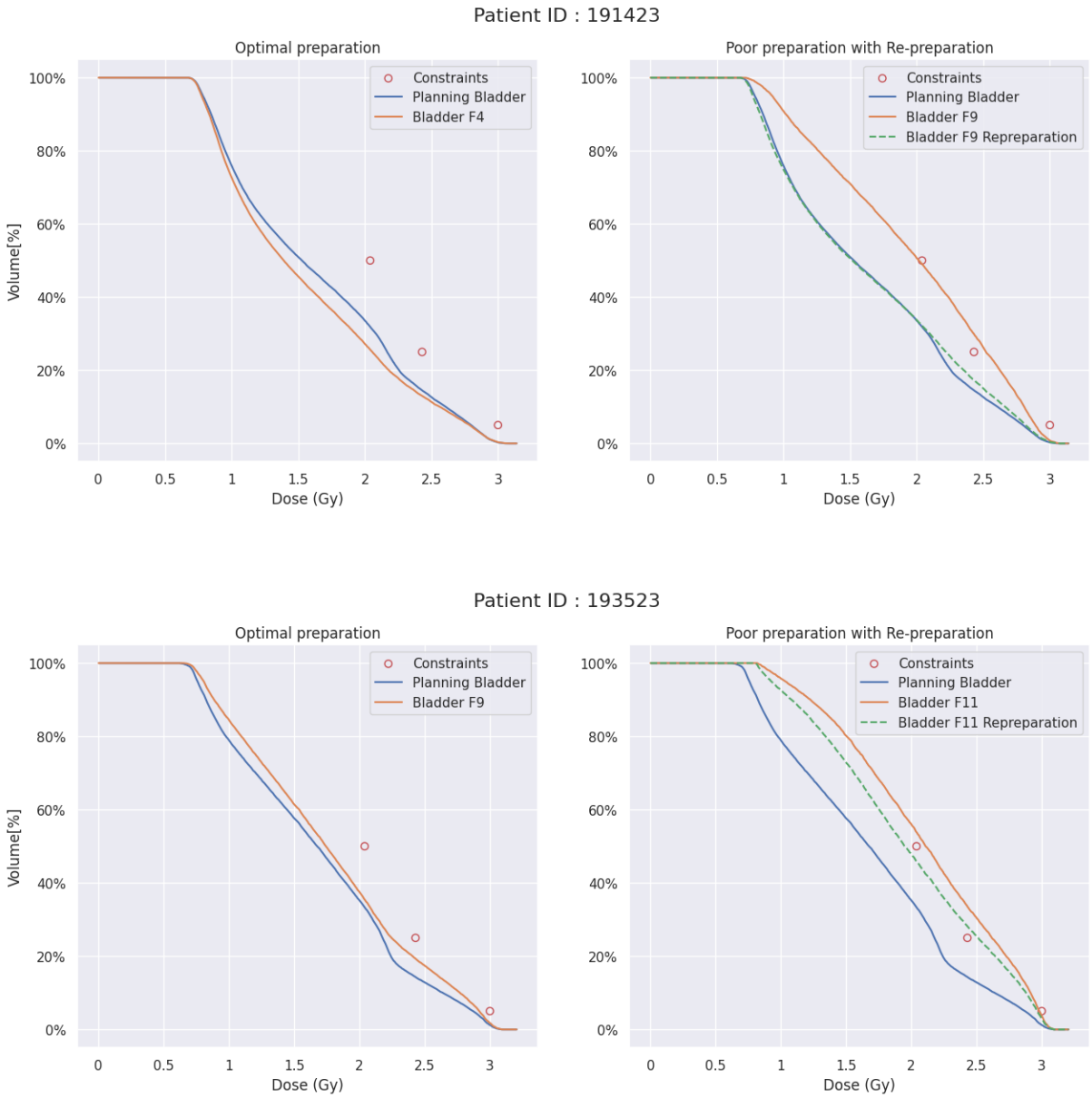

Figure 4.1: Comparison of bladder DVHs between simulation (planning) preparations and optimal preparations (left subfigures) and poor preparations, including re-preparations (right subfigures). The fraction number is mentioned in each subfigure legend.

All patients, except for patient 010924, showed drastic dose volume differences between their planning preparation and their poor preparation[1] in both low and high dose regions. Re-preparations significantly reduced these differences in those delivered fractions. For most patients, Initial planning preparations could have been improved to match the optimal preparation (See figure **??**).

Dose volume metrics indicated an average inter-fraction difference between planning preparations and poor preparations. An increase of 18.48% in bladder volume recieving 2.04 Gy ($V_{2.04\%}$), 13.68% in bladder volume recieving 2.43 Gy ($V_{2.43\%}$) and 1.2% bladder volume recieving 3 Gy ($V_{3\%}$).

[1]Poor preparation refers to the worst preparation in terms of dose-volume metrics throughout the whole subsequent treatments

Patient ID	Bladder DVH metrics of preparations for a single fraction in %								
	Simulation(Planning)			Poor			Poor with Re-preparation		
	$V_{2.04\%}$	$V_{2.43\%}$	$V_{3\%}$	$V_{2.04\%}$	$V_{2.43\%}$	$V_{3\%}$	$V_{2.04\%}$	$V_{2.43\%}$	$V_{3\%}$
011324	50.4	31.61	3.33	88.61	65.33	8.41	56.78	35.8	5.16
009224	37.27	20.65	1.64	58.24	35.82	0.0	/	/	/
022324	38.1	23.0	2.7	60.55	37.53	4.3	/	/	/
025124	21.73	13.9	2.2	23.66	9.69	0.22	26.0	16.85	2.65
002424	20.51	13.88	2.95	51.65	35.16	6.76	38.44	26.58	5.56
009524	14.14	9.24	1.35	25.58	15.27	1.21	/	/	/
010924	11.38	7.83	1.8	14.66	10.31	2.68	/	/	/
186523	27.66	10.53	0.82	45.32	24.67	2.26	/	/	/
191423	31.89	14.5	0.28	49.05	29.92	0.8	32.21	17.29	0.42
193523	33.31	14.3	1.22	53.84	33.54	3.64	45.87	28.13	2.9
Mean	28.64	15.94	1.83	47.12	29.62	3.03	39.06	24.93	3.34

Table 4.1: Comparison of Bladder DVH metrics ($V_{2.04\%}$, $V_{2.43\%}$, $V_{3\%}$) at designated fractions in figure **??**. $V_{x\%}$ represents a percentage of the bladder volume that receives dose x(Gy)

Patient ID	Bladder Volume of preparations in cc			
	Simulation (Planning)	Optimal	Poor	Poor with re-preparation
011324	253.84	261.81	86.0	139.66
009224	240.7	349.2	98.54	/
022324	288.13	301.64	161.4	/
025124	405.07	596.67	200.94	329.38
002424	261.54	726.93	76.33	102.89
009524	502.45	594.29	189.41	/
010924	647.78	839.27	421.76	/
186523	386.1	306.46	135.71	/
191423	352.19	295.77	127.46	242.62
193523	290.6	189.2	96.4	121.06
Mean	342.84	447.02	159.395	187.122

Table 4.2: Comparison of bladder volumes at designated fractions in figure **??**

Comparing the bladder volumes of different preparations, the results indicated a mean inter-fraction difference of 183.445 cc (53.5%) between planning preparations and poor preparations, showing a significant decrease in bladder volume. Re-preparations helped increase the bladder volume by 27.72cc (8.09%). However, optimal preparations had an average increase of 104.18cc (30.39%) in bladder volume.

These findings provide a foundation for the next section, where their link will explored.

4.1.2 Correlation between dose and volume

The exponential regression model that was fit to the data indicated a good R^2 score of 77.33% indicating that 77.33% of the variance in the mean dose received by the bladder can be explained by the relative bladder volume. The regression model is given by the equation :

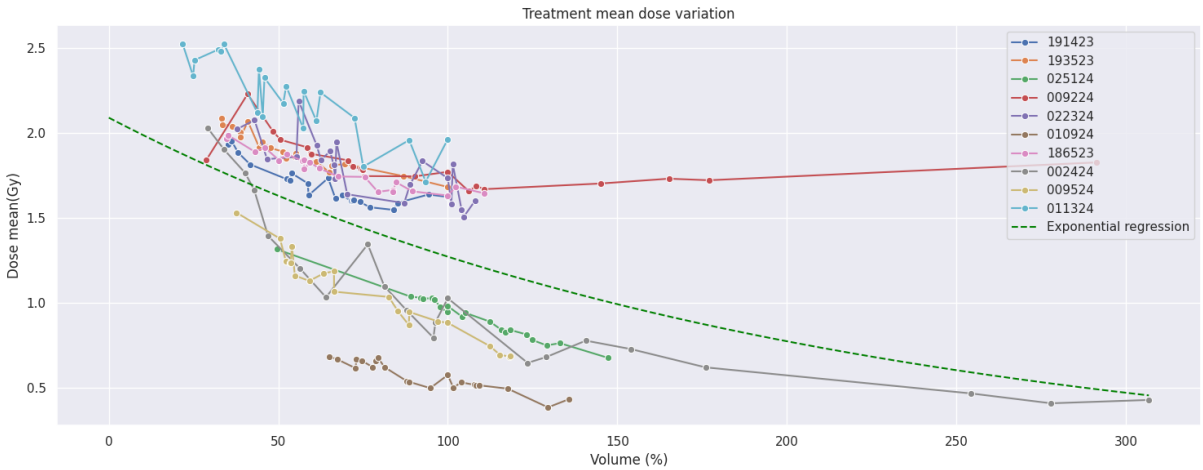

Figure 4.2: Comparison of the mean dose received by the bladder in each treatment session with the relative volume (relative to the planning bladder volume) of all patients, including an exponential regression.

$$Y = ae^{bX} \tag{4.1}$$

where :

- Y represents the mean dose received by the bladder,
- X represents the relative bladder volume,
- a and b are the model parameters.

The estimated parameters for the model are:

- $a = 2.091854$
- $b = -0.004964$

The parameter b indicates the rate of decrease in the mean dose with increasing relative bladder volume. The negative value of b suggests that as the relative bladder volume increases, the mean dose received by the bladder decreases exponentially.

4.1.3 Summation DVH Comparison

Patient ID : 011324

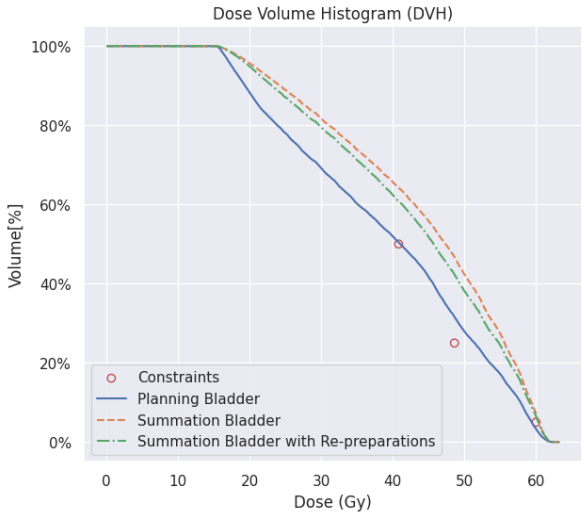

	Planning	Summation	Summation with Re-preparations	Constraints
V60%	3.33	7.15	6.47	<5%
V48.6%	31.61	46.7	42.32	<25%
V40.8%	50.4	64.19	60.81	<50%

Patient ID : 009224

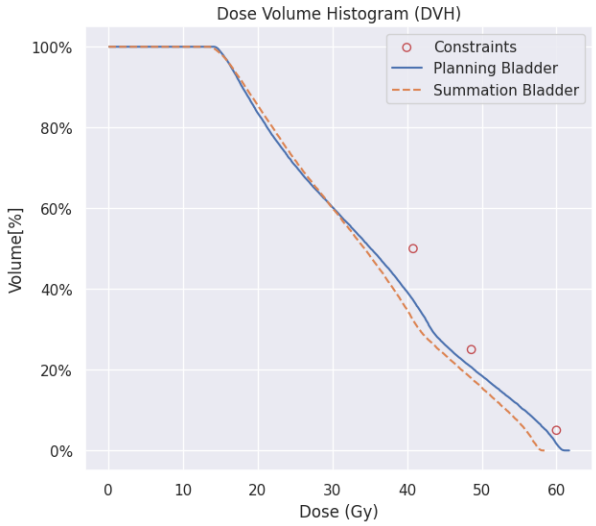

	Planning	Summation	Constraints
V60%	1.64	0.0	<5%
V48.6%	20.65	17.9	<25%
V40.8%	37.27	32.23	<50%

Patient ID : 022324

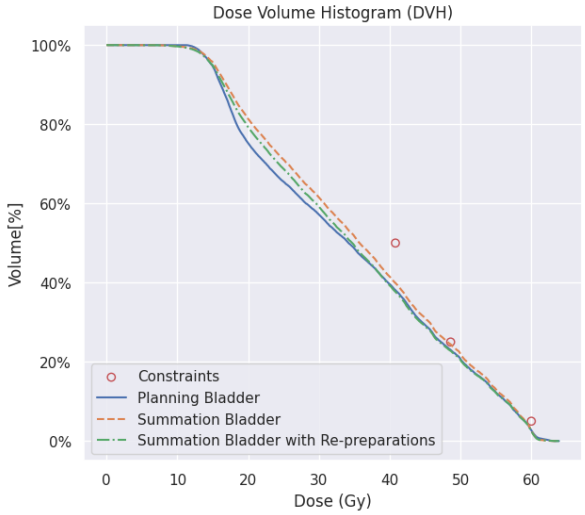

	Planning	Summation	Summation with Re-preparations	Constraints
V60%	2.7	2.61	2.46	<5%
V48.6%	23.0	24.42	22.77	<25%
V40.8%	38.1	39.92	37.7	<50%

Patient ID : 025124

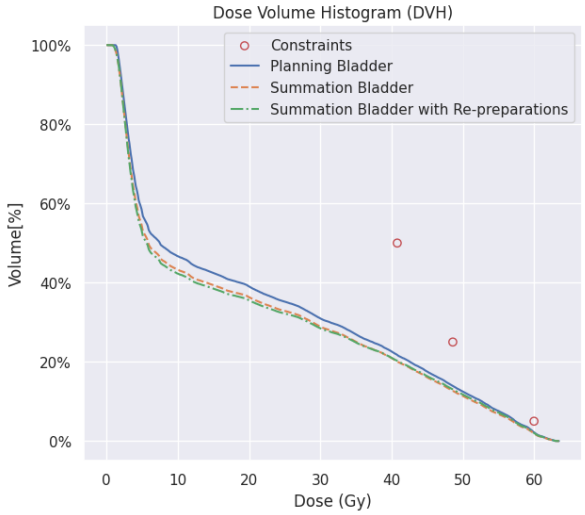

	Planning	Summation	Summation with Re-preparations	Constraints
V60%	2.2	1.92	2.04	<5%
V48.6%	13.9	12.66	13.02	<25%
V40.8%	21.73	20.1	20.22	<50%

Patient ID : 002424

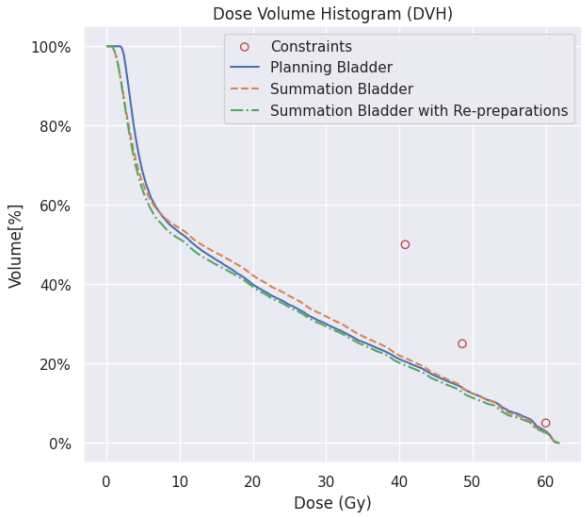

	Planning	Summation	Summation with Re-preparations	Constraints
V60%	2.95	2.77	2.56	<5%
V48.6%	13.88	13.91	12.7	<25%
V40.8%	20.51	21.35	19.55	<50%

Patient ID : 009524

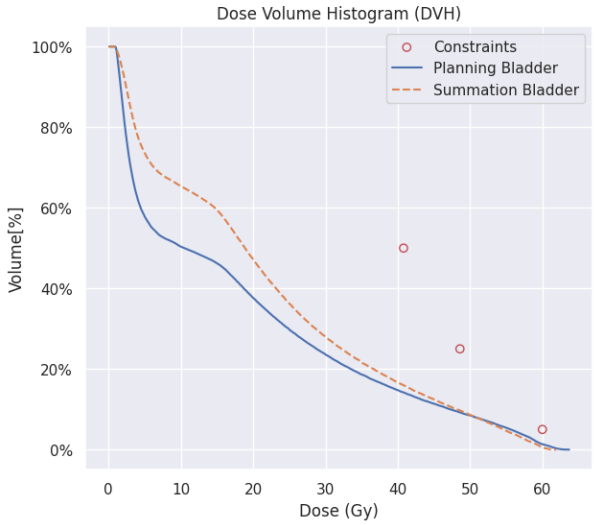

	Planning	Summation	Constraints
V60%	1.35	0.59	<5%
V48.6%	9.24	9.74	<25%
V40.8%	14.14	16.0	<50%

Patient ID : 010924

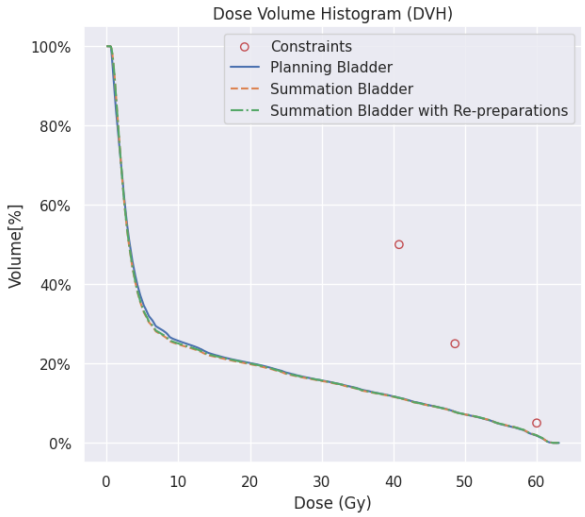

	Planning	Summation	Summation with Re-preparations	Constraints
V60%	1.8	1.87	1.87	<5%
V48.6%	7.83	7.75	7.79	<25%
V40.8%	11.38	11.27	11.34	<50%

Patient ID : 186523

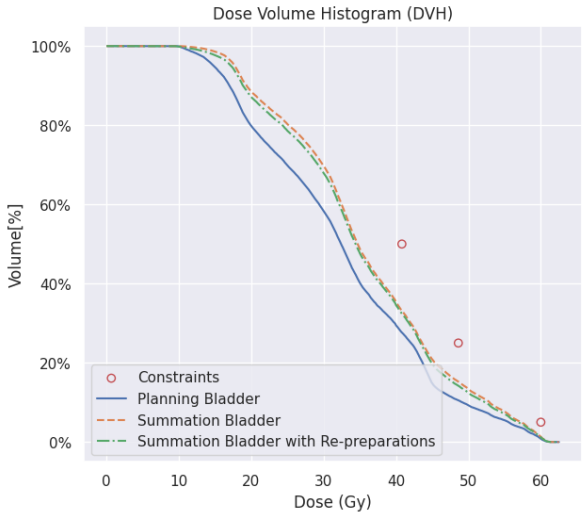

	Planning	Summation	Summation with Re-preparations	Constraints
V60%	0.82	1.31	1.22	<5%
V48.6%	10.53	15.24	14.21	<25%
V40.8%	27.66	33.15	32.44	<50%

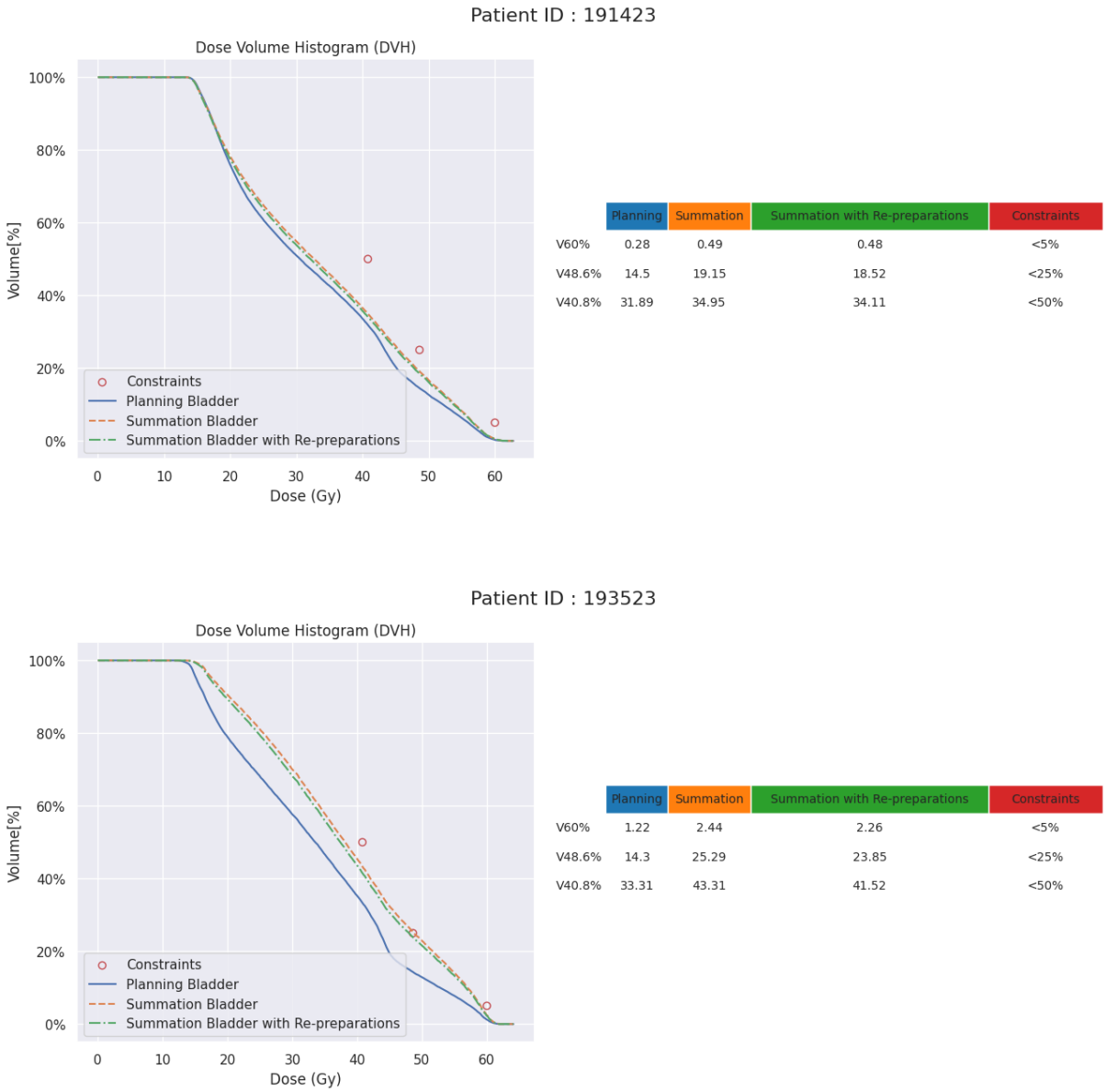

Figure 4.3: Comparison of bladder DVHs between simulation (planning), summed DVHs of treatment sessions without re-preparations, and summed DVHs of treatment sessions with re-preparations. The right subfigure includes a table of metrics for the mentioned DVHs.

6 out of 10 patients had DVH metrics exceed the planning and 2 of them exceeded the constraints. 3 patients out of 10 had receding metrics. Patient 002424 had crossing DVH metrics (These metrics consider only high dose region).

Patient 193523 re-preparations contributed to lowering metrics below the constraints.

4.1.4 Impact of poor simulation preparations

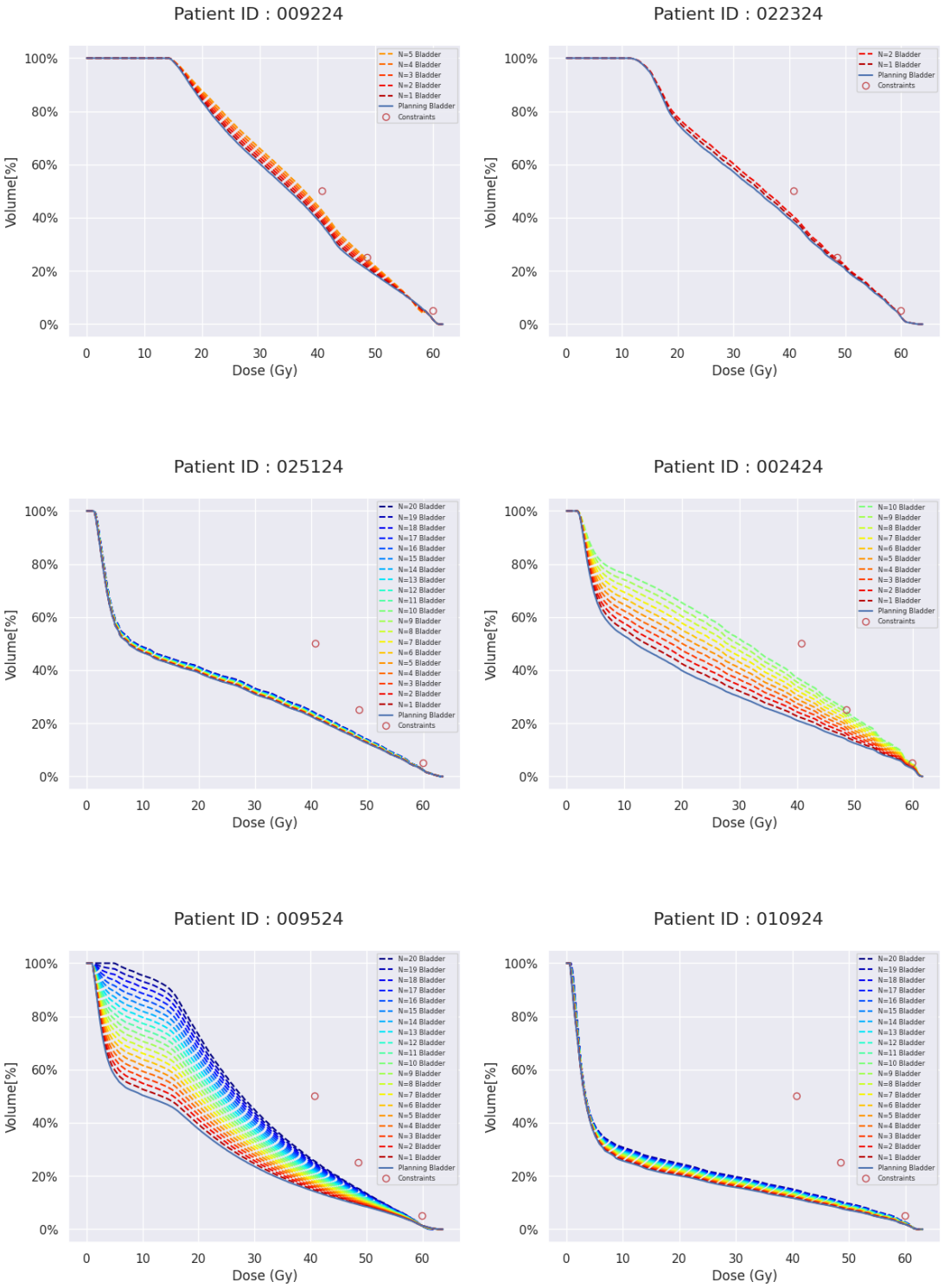

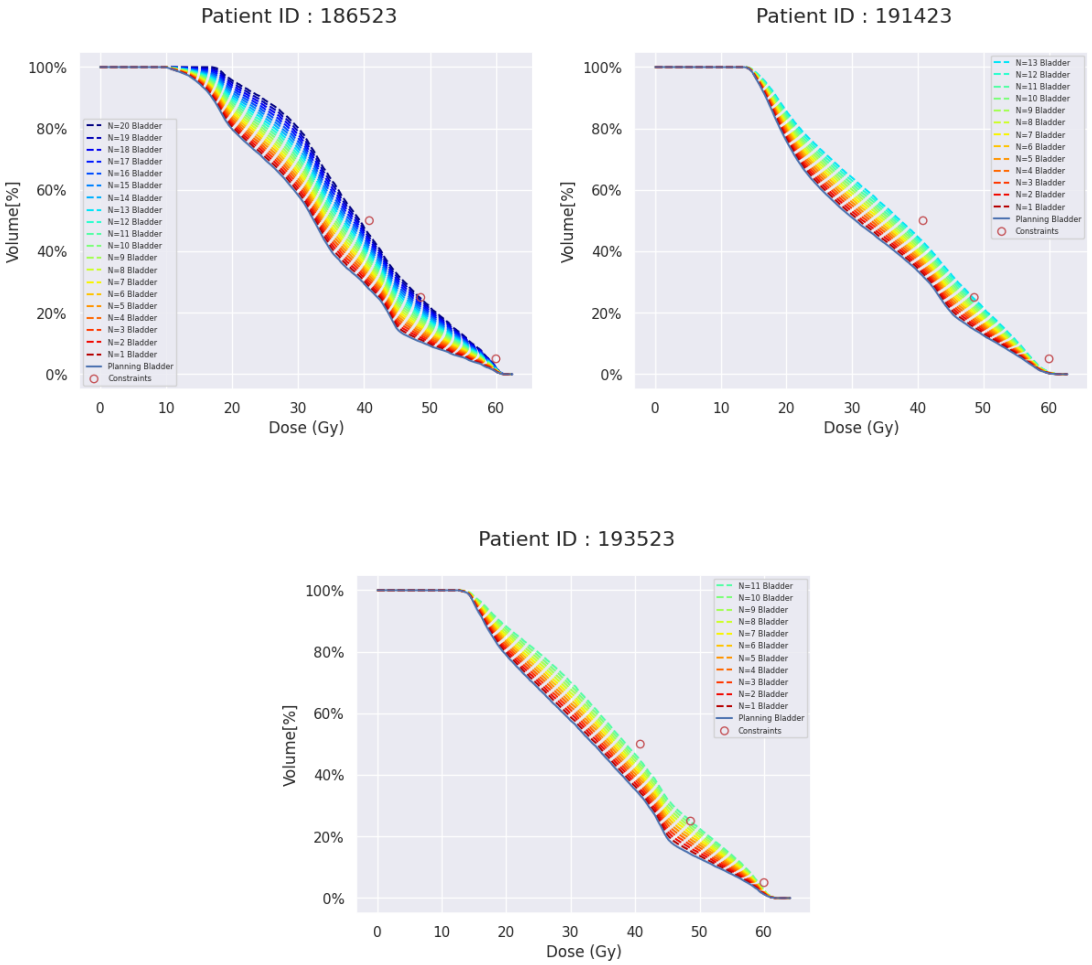

Figure 4.3: Greatest possible number of poor preparations allowed before exceeding the constraints for each planning. This was achieved by summing planning DVHs with N number of poor preparations DVHs.

Patient ID	Planning Bladder Volume in cc	Number of possible poor preparations
011324	253.84	0
009224	240.7	5
022324	288.13	2
025124	405.07	20
002424	261.54	10
009524	502.45	20
010924	647.78	20
186523	386.1	20
191423	352.19	13
193523	290.6	11

Table 4.3: Relationship between planning bladder volume and the number of possible poor preparations for each patient.

The results (Table 4.3, Figure **??** and 4.4) show a linear increase in the number of acceptable poor preparations versus the planning bladder volume. This trend continues until reaching the planning bladder volume of 398.61 cc, at which point all poor preparations become acceptable for the entire hypofractionated treatment course.

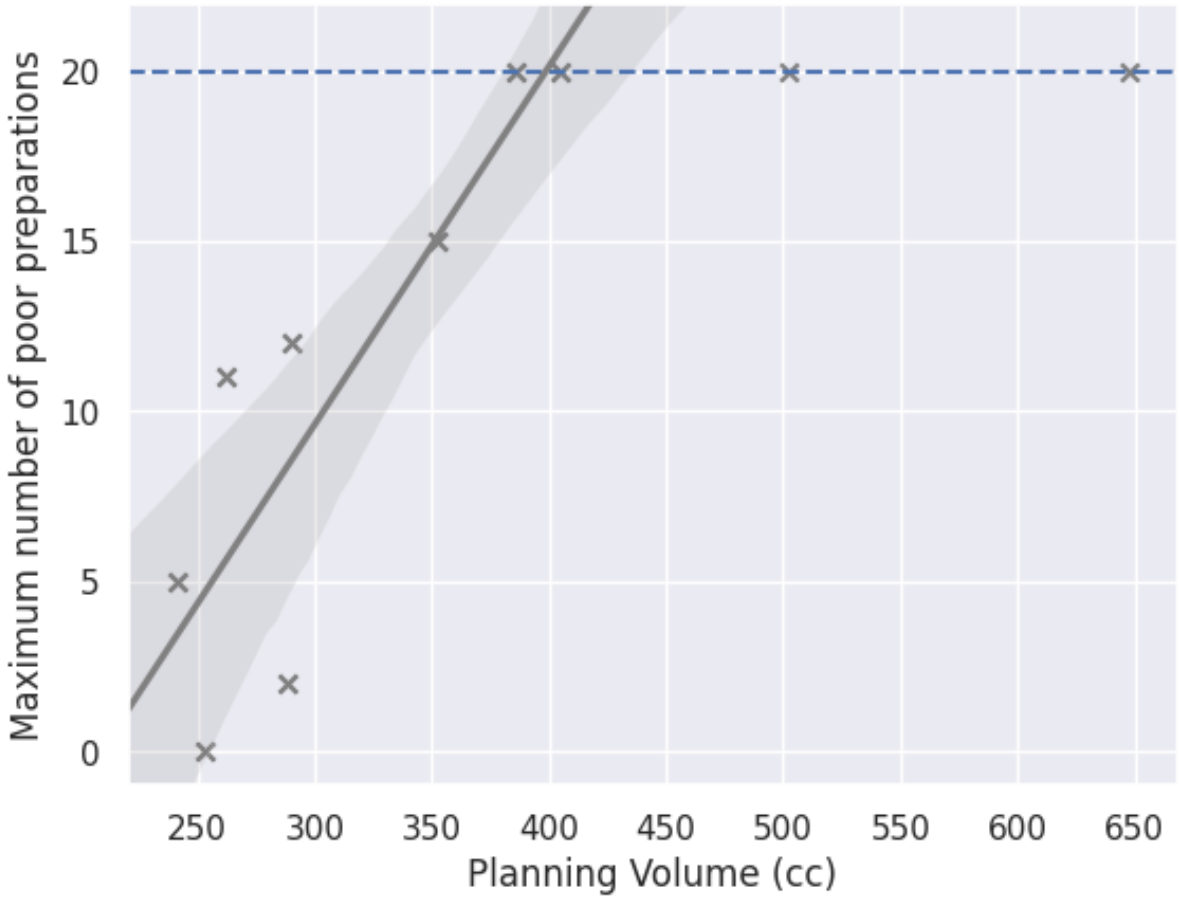

Figure 4.4: Scatterplot showing the relationship between maximum number of possible poor preparations and planning bladder volume with a linear regression. The horizontal dashed line is number of fractions in a hypofractionated therapy and the goal set to achieve.

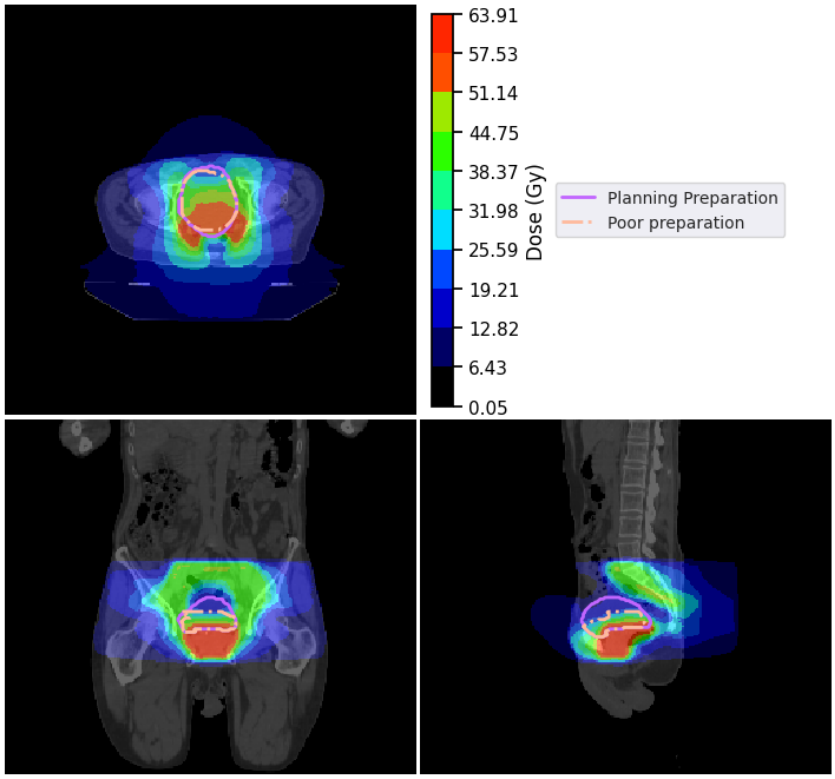

(a) Patient 022324 with Planning Bladder Volume : 288.13 cc

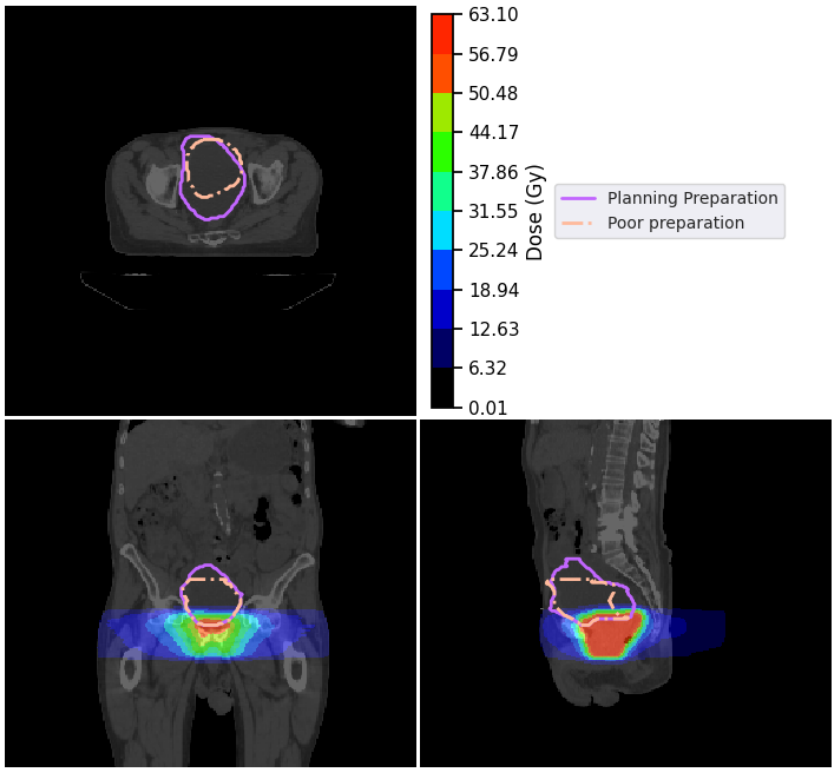

(b) Patient 010924 with Planning Bladder Volume : 647.78 cc

Figure 4.5: Isodose comparison (in transversal, coronal, and sagittal views) between low bladder volume and high bladder volume in planning preparation and poor preparations

4.2 Second study case : Patients survey

ID	Age	Fraction	Last Discharge (Hrs)	Last Drink (Hrs)	Drink Quantity (L)	Re-prepared
0071 24	75	16 / 38	0.52	0.77	1	N
1877 23	72	35 / 38	0.17	1.58	1.5	Y
1885 23	74	28 / 33	0.72	0.72	0.5	N
1880 23	77	38 / 38	8.17	2.67	1	N
1634 23	61	32 / 33	/	/	0.5	N
0207 24	80	4 / 20	/	1.47	1	N
1890 23	79	27 / 38	2.63	0.63	1.5	N
0071 24	75	21 / 38	/	/	1	N
0010 24	72	23 / 33	3.25	0.75	1.5	N
1863 23	76	17 / 19	3.5	1.08	0.5	N
1821 23	84	/	/	12	2	N
1634 23	61	/	/	/	0.5	N
0150 24	71	12 / 37	2.88	4.38	1.5	N
0185 24	67	7 / 20	14.03	12.45	1	N
0223 24	74	Planning			1	N
0092 24	85	17 / 20	0.5	0.1	0.5	N
1353 23	75	22 / 38	0.5	0.4	0.5	N
0201 24	80	8 / 20	/	1	1	N
1863 23	76	38 / 38	/	/	/	Y
0131 24	72	17 / 38	2	1.75	1.25	N
0071 24	75	25 / 38	4	0.25	1.25	N
0185 24	65	11 / 20	0	0	2	N
0090 24	73	10 / 19	1	0.1	1.25	N
1885 23	74	33 / 38	0.1	0	1	N
0150 24	66	30 / 38	/	/	2.5	N
0017 24	66	30 / 38	1	1	1.5	N
0089 24	75	20 / 38	1	2	2.5	N
0084 24	65	25 / 38	5	0.8	0.5	N

Table 4.4: Gathered information from patients survey

ID	Last Discharge (Hrs)	Last Drink (Hrs)	Drink Quantity (L)	Bladder Volume (cc)
0223 24	/	1	1	266.45
0092 24	0.5	0.1	0.5	170.06

Table 4.5: Comparison between gathered survey informations and real bladder volume.

From table 4.4 and 4.5, it is evident that the sample size was smaller than anticipated. This reduction was primarily due to missing data on real bladder volumes. Specifically, out of the expected 28 samples, only 2 had complete data on bladder volumes, resulting in a smaller sample size for analysis.

ID	Fraction	Volume Difference (cc)	Duration (min)	Filling rate(cc/min)
1935 23	4	116.03	104	1.12
1935 23	5	86.58	73	1.19
1935 23	11	24.65	41	0.60
1914 23	9	115.13	40	2.88
0251 24	9	128.31	39	3.29
0223 24	6	186.28	64	2.91
0223 24	7	30.29	98	0.31
0223 24	18	60.36	75	0.80
1865 23	1	443.47	157	2.82
1865 23	2	23.05	129	0.18
1865 23	3	84.82	107	0.79
1865 23	7	65.90	110	0.60
1865 23	12	81.39	74	1.10

Table 4.6: Relationship between the difference in recorded bladder volume during treatment preparation and re-preparation and the duration.

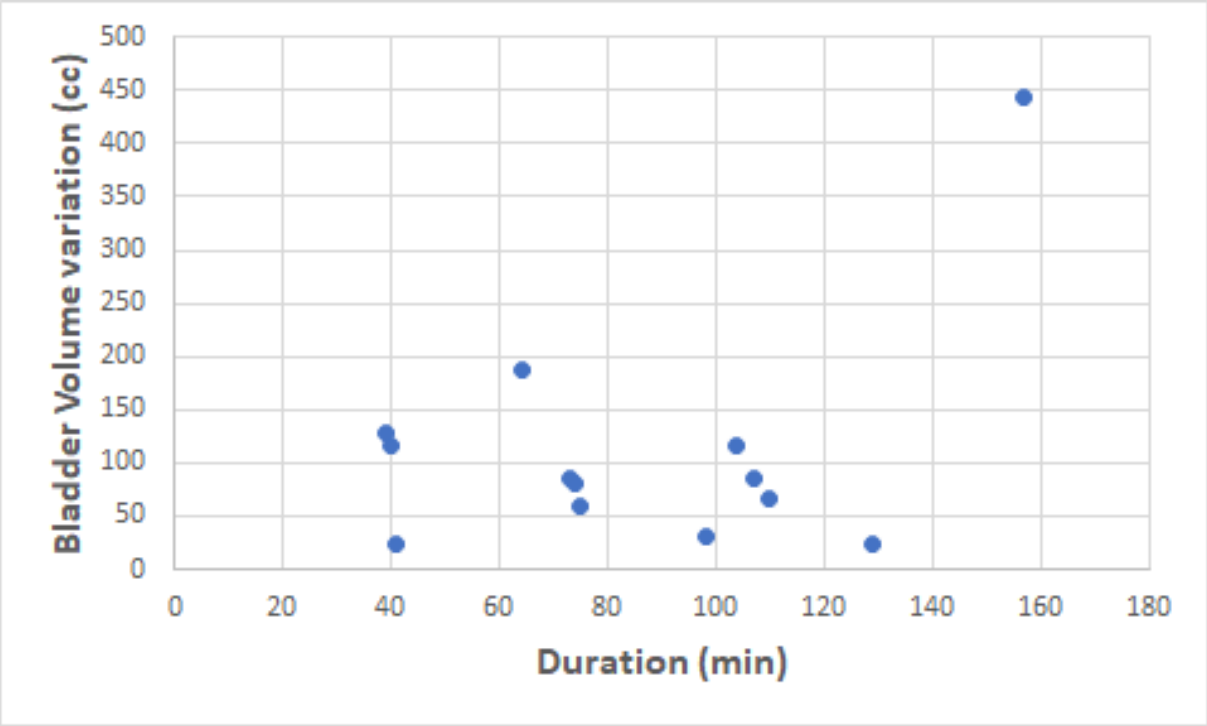

Figure 4.6: Scatterplot of Volume difference between two preparations versus Duration.

Figure 4.6 showed a high variance with an R^2 score of 0.1724 and did not align with the overall expected pattern.

Chapter 5. Discussions and conclusion

5.1 Discussion of results

Fractions with poor preparations (that is preparations with higher DVH metrics) tend to have smaller bladder volumes. On the contrary, optimal preparations are associated with larger bladder volumes. This can be attributed to the anatomy of the bladder, which contracts to a lower position in the body, closer to the prostate (PTV), thus becoming more contained within the isodose curve. Some patients exhibited lower metrics in the poor preparations within the high-dose region due to the bladder's anatomy and the specific approach used to plan the treatment.

This relationship is further seen in the second section, where an exponential decrease in mean dose with increasing bladder volume is observed. Re-preparations greatly optimized the overall difference for almost all patients who had re-preparations done on these fractions. However, in the case of summation dose, infrequent re-preparations had significantly less impact on the total delivered dose, except for one patient (193523), where the re-preparations prevented the summation dose from exceeding the constraints.

Summation DVHs also showed that patients exhibited contrasting results, with some having their DVHs exceed the planned DVHs, while others had reduced DVHs. This variation is primarily due to the fact that bladder volume depends strictly on the patient's commitment and their body's metabolism. The latter one led to analyzing the impact of the poor preparations on the overall summed dose. The number N_{prep}, Greatest possible number of poor preparations allowed for a single patient, is closely linked to the planning bladder volume. Notably, a larger bladder volume during planning permits a higher number of poor preparations before surpassing the dose constraints. The value N_{prep} reached a maximum at around 400 cc, indicating that treatment can proceed with the poorest preparation scenario (where all subsequent treatment DVHs mirror that of a poor preparation) without going above the constraints. Taking into account the accuracy of the treatment planning, as demonstrated with patient 011324, where the patient's bladder volume already exceeded the constraints during planning.

This is demonstrated in figure 4.5 by comparing the planning bladder volume and how the bladder in poor preparations is contained by the isodose. It is evident in the coronal and sagittal views that in cases of poor preparation, where the planning bladder volume is low, the isodose spreads

across other areas. As the result of that, the center of mass of the bladder is still contained within the isodose as seen in the transversal view. In contrast, when the planning bladder volume is high, the isodose is well-defined by the planning bladder structure and does not spread to other areas.

In the second study case, patients were randomly selected. As a result, not all bladder contours matched with the surveyed patients, leading to missing data and a small sample size for analysis. This also applies to calculating the filling rate of the bladder as seen in table 4.6, since each patient have a variation to be studied. This study also revealed that not all patients were reliable and consistent towards the preparation.

5.2 Conclusion

The results demonstrated that all well-prepared patients met the treatment constraints, and the dose received by the bladder directly correlated with it's volume. Other findings showed that thorough bladder preparation before planning is crucial, as it significantly impacts the effectiveness and accuracy of subsequent treatments.

5.3 Future work

To further enhance the findings of this research, several steps are recommended. Firstly, increasing the sample size in both study cases will improve the statistical power and generalizability of the results.

For the first study case, it is important to investigate the impact of poor preparations in non-hypofractionated treatments. This will provide valuable insights into how preparation quality affects treatment efficacy in different radiotherapy regimens.

In the second study case, a meticulous approach should be taken by contouring the bladders of all surveyed patients to prevent missing data. Additionally, patients should be surveyed throughout all their subsequent treatments. This comprehensive follow-up will allow for a thorough assessment of the dose-response relationship and long-term patient outcomes, ultimately leading to improved treatment protocols and patient care.

Acknowledgements

We would like to express our deepest gratitude to our supervisor, Mr. Ahmed SIDIMOUSSA, for their unwavering support, guidance, and encouragement throughout this research. Their insightful feedback and dedication to our project were instrumental in its completion.

We also extend our heartfelt thanks to the entire team at SIDI Abellah ONCOLOGY CENTER for their invaluable assistance and collaboration.

Lastly, we are profoundly grateful to our families and friends for their constant support, patience, and understanding during this journey.

Thank you all for being with us every step of the way.

Bibliography

[1] International Atomic Energy Agency. Diagnostic Radiology Physics. Text, International Atomic Energy Agency, 2014.

[2] Kristina Andersson. Evaluation of uncertainties in sub-volume based image registration: Master of science thesis in medical radiation physics. Master's thesis, Umeå University, Faculty of Science and Technology, Department of Physics., 2010.

[3] Giampaolo Bolzicco, M. Favretto, Ninfa Satariano, Enrico Scremin, C. Tambone, and Andrea Tasca. A single-center study of 100 consecutive patients with localized prostate cancer treated with stereotactic body radiotherapy. *BMC urology*, 13:49, October 2013.

[4] P. Catuzzo, F. Zenone, S. Aimonetto, A. Peruzzo, V. Casanova Borca, M. Pasquino, P. Franco, M. R. La Porta, U. Ricardi, and S. Tofani. Technical note: Patient-specific quality assurance methods for TomoDirect ™ whole breast treatment delivery: TomoDirect ™ whole breast DQA with diode arrays. *Medical Physics*, 39(7Part1):4073–4078, June 2012.

[5] Byungchul Cho. Intensity-modulated radiation therapy: A review with a physics perspective. *Radiation Oncology Journal*, 36(1):1–10, March 2018.

[6] Sonya Collins. Types of Prostate Cancer. https://www.webmd.com/prostate-cancer/types-prostate-cancer.

[7] Mary Weinstein Dunn and Meredith Wallace Kazer. Prostate Cancer Overview. *Seminars in Oncology Nursing*, 27(4):241–250, November 2011.

[8] Benedick A. Fraass. The development of conformal radiation therapy. *Medical Physics*, 22(11):1911–1921, November 1995.

[9] Pierfrancesco Franco, Paola Catuzzo, Domenico Cante, Maria Rosa La Porta, Piera Sciacero, Giuseppe Girelli, Valeria Casanova Borca, Massimo Pasquino, Gianmauro Numico, Santi Tofani, Teodoro Meloni, Umberto Ricardi, and Franca Ozzello. TomoDirect: An efficient means to deliver radiation at static angles with tomotherapy. *Tumori Journal*, 97(4):498–502, July 2011.

[10] Robert Jeraj, Thomas R. Mackie, John Balog, Gustavo Olivera, Dave Pearson, Jeff Kapatoes, Ken Ruchala, and Paul Reckwerdt. Radiation characteristics of helical tomotherapy. *Medical Physics*, 31(2):396–404, February 2004.

[11] Glenn F. Knoll. *Radiation Detection and Measurement*. John Wiley, Hoboken, N.J, 4th ed edition, 2010.

[12] Katja M. Langen, Niko Papanikolaou, John Balog, Richard Crilly, David Followill, S. Murty Goddu, Walter Grant III, Gustavo Olivera, Chester R. Ramsey, and Chengyu Shi. QA for helical tomotherapy: Report of the AAPM Task Group 148a). *Medical Physics*, 37(9):4817–4853, 2010.

[13] T. Rock Mackie, Timothy Holmes, Stuart Swerdloff, Paul Reckwerdt, Joseph O. Deasy, James Yang, Bhudatt Paliwal, and Timothy Kinsella. Tomotherapy: A new concept for the delivery of dynamic conformal radiotherapy. *Medical Physics*, 20(6):1709–1719, 1993.

[14] Michael T. Milano, Lawrence B. Marks, and Louis S. Constine. Survivorship and Late Effects. In *Clinical Radiation Oncology*, pages 239–256. Elsevier, 2012.

[15] Claire H. Pernar, Ericka M. Ebot, Kathryn M. Wilson, and Lorelei A. Mucci. The Epidemiology of Prostate Cancer. *Cold Spring Harbor Perspectives in Medicine*, 8(12):a030361, December 2018.

[16] Cheng B. Saw, Leah Katz, Carol Gillette, and Lawrence Koutcher. 3D treatment planning on helical tomotherapy delivery system. *Medical Dosimetry*, 43(2):159–167, 2018.

[17] Hyuna Sung, Jacques Ferlay, Rebecca L. Siegel, Mathieu Laversanne, Isabelle Soerjomataram, Ahmedin Jemal, and Freddie Bray. Global Cancer Statistics 2020: GLOBOCAN Estimates of Incidence and Mortality Worldwide for 36 Cancers in 185 Countries. *CA: a cancer journal for clinicians*, 71(3):209–249, May 2021.

[18] Lei Xing, Brian Thorndyke, Eduard Schreibmann, Yong Yang, Tian-Fang Li, Gwe-Ya Kim, Gary Luxton, and Albert Koong. Overview of image-guided radiation therapy. *Medical Dosimetry*, 31(2):91–112, June 2006.